

Implications of a Froissart bound saturation of γ^*p deep inelastic scattering. Part I. Quark distributions at ultra small x .

Martin M. Block*

Department of Physics and Astronomy, Northwestern University, Evanston, IL 60208

Loyal Durand†

Department of Physics, University of Wisconsin, Madison, WI 53706

Phuoc Ha‡

Department of Physics, Astronomy and Geosciences, Towson University, Towson, MD 21252

Douglas W. McKay§

Department of Physics and Astronomy, University of Kansas, Lawrence, KS 66045

(Dated: February 26, 2013)

We revisit arguments that the structure function $F_2^{\gamma p}(x, Q^2)$ for deep inelastic γ^*p scattering is hadronic in nature, similar to vector dominance for real γp scattering. Thus, like all other known hadronic scattering, including γp , the growth of $F_2^{\gamma p}(x, Q^2)$ is limited by the Froissart bound at high hadronic energies, giving a $\ln^2(1/x)$ bound as Bjorken $x \rightarrow 0$. The same bound holds for the individual quark distributions that contribute to $F_2^{\gamma p}$. In earlier work, we presented a very accurate global fit to the combined HERA data based on a fit function which respects the Froissart bound at small x , and is equivalent in its x dependence to the function used successfully to describe all high energy hadronic data. We discuss the extrapolation of the fit to the values of x down to $x = 10^{-14}$ encountered in the calculation of neutrino cross sections at energies up to $E_\nu = 10^{17}$ GeV, an extrapolation of a factor of ~ 3 beyond the HERA region in the natural variable $\ln(1/x)$. We show how the results can be used to derive the relevant quark distributions. These distributions do not satisfy the “wee parton” condition, that they all converge toward a common distribution $xq(x, Q^2)$ at small x and large Q^2 which is just a multiple of $F_2^{\gamma p}$, but still give results for the dominant neutrino structure function $F_2^{\nu(\bar{\nu})}$ which differ only slightly from those obtained assuming that the wee parton limit holds.

PACS numbers: 12.38.Bx, 12.38.-t, 13.60.Hb

I. INTRODUCTION

The experimental program at HERA, the electron-proton collider at DESY, probed deep inelastic scattering (DIS) at small values of the Bjorken variable x , given in terms of the proton momentum p and the electron momentum transfer q in the scattering by $x \approx Q^2/2p \cdot q$. The measurements covered the range 10^{-6} to 10^{-1} in x , with a corresponding range from 1 GeV² to 5000 GeV² for the virtuality $Q^2 = -q^2$. The results of the extensive measurements by the H1 and ZEUS detector groups show that the structure function $F_2^{\gamma p}(x, Q^2)$ rises rapidly as x decreases with Q^2 fixed.

A series of papers over the past few years [1–4] made the case that the reduced cross section in DIS, basically the structure function $F_2^{\gamma p}(x, Q^2)$, is hadronic in nature and satisfies a saturated Froissart bound, implying that $F_2^{\gamma p}(x, Q^2) \rightarrow \text{constant} \times \ln(1/x)^2$ for $x \rightarrow 0$ with Q^2 fixed. The basic argument is that the structure function $F_2^{\gamma p}$ is determined by the total cross section of an off-shell gauge boson γ^* on the proton at a γ^*p center-of-mass energy squared $W^2 = \hat{s}$, where $\hat{s} = (p + q)^2$ is the usual Mandelstam variable, and is thus subject through analyticity and unitarity constraints to the saturated Froissart bound on total hadronic cross sections $\sigma(\hat{s}) \rightarrow \sigma_0 \log^2 \hat{s}$ as $\hat{s} \rightarrow \infty$. The picture is compelling in light of its success in describing hadron-hadron and photon-hadron total cross sections over many orders of magnitude with the same basic functional form [5]. Moreover, its *predictions* for the proton-proton and proton-air cross sections at the LHC [6–8] and the Pierre Auger Observatory [9], respectively, are confirmed by these new high energy experiments [10–12].

*Electronic address: mblock@northwestern.edu

†Electronic address: ldurand@hep.wisc.edu; Mailing address: 415 Pearl Ct., Aspen, CO 81611

‡Electronic address: pdha@towson.edu

§Electronic address: dmckay@ku.edu

In this paper, we investigate the implications of this bounded behavior for the ultra-small x , large Q^2 limit of the quark distributions in the proton using our recent Froissart-bounded fit to the combined HERA data. We show that the individual quark distributions can be derived to reasonable accuracy directly from $F_2^{\gamma p}$, and present the results obtained using the extrapolation of our fit to ultra-small x . The extrapolation should be reliable: the fit function becomes a simple quadratic in the natural variable $v = \ln(1/x)$ with well-determined coefficients for x small or v large, and the extrapolation necessary to reach $x = 10^{-14}$ ($v = 32.2$) involves only a factor ~ 3 increase in v from the upper values attained in the HERA region.

In earlier calculations [3, 4] of ultra high energy (UHE) neutrino-nucleon cross sections, it was assumed that the quark distributions could be treated in a “wee parton” limit in which the individual quark distributions all converge to a common quark distribution $xq(x, Q^2)$ at large Q^2 and small x . This allowed the replacement of individual quark distributions in the neutrino cross sections by xq , given in terms of $F_2^{\gamma p}$ by $xq = F_2^{\gamma p} / \sum_i e_i^2$, where the e_i are the quark charges and the sum runs over the active quarks and antiquarks. We show here that the wee parton condition is *not* satisfied by the quark distributions determined directly from our fit to $F_2^{\gamma p}$. However, the relations between $F_2^{\gamma p}$ and the corresponding charged- and neutral-current structure functions $F_2^{\nu(\bar{\nu})}$ and $F_0^{\nu(\bar{\nu})}$ in neutrino and antineutrino scattering which were derived using the wee parton assumption continue to hold to high accuracy.

In Part II of this work, the companion paper [13] to this one, we extend our earlier calculations of UHE charged- and neutral current neutrino-nucleon cross sections $\sigma_{CC}^{\nu}(E_\nu)$ and $\sigma_{NC}^{\nu}(E_\nu)$ up to $E_\nu = 10^{17}$ GeV, currently the highest energies where there are experimental bounds on cosmic neutrino fluxes [14, 15]. These calculations require input at large Q^2 ($Q^2 \gtrsim 10^4$) and small x , down to $x \sim 10^{-14}$. The results presented here are highly significant for that work. The results in Part II extend our earlier work both by pushing the neutrino energy higher, to $E_\nu = 10^{17}$ GeV, and by including the contributions of the b quark.

The present paper is organized as follows. In Sec. II, we develop our arguments with respect to the relevance of the Froissart bound and its consequences for the form used in our parameterization of the small- x HERA data for $F_2^{\gamma p}(x, Q^2)$. We then summarize the results of our fit [16] to the combined HERA data [17], and list the parameters, their errors and the significance of the fit. In Sec. III A, we discuss the derivation of the *individual* small x quark distributions from our analytic fit to $F_2^{\gamma p}(x, Q^2)$. This requires information on the singlet quark distribution $F_s(x, Q^2)$ which can be expressed in terms of a “bare” structure function $F_{20}^{\gamma p}$ and a set of non-singlet quark distributions. We show in an Appendix how $F_{20}^{\gamma p}$ can be related readily to our fit to $F_2^{\gamma p}$, and develop simple results for the effect of QCD evolution on the non-singlet distributions in Sec. III B. Our results for quark distributions at ultra-small x are given in Sec. IV A. We discuss their implications with respect to the wee parton picture and neutrino cross sections in Sec. IV B, where we show that $F_2^{\nu(\bar{\nu})}$, the dominant neutrino structure function, can be expressed directly in terms of $F_2^{\gamma p}$ to good approximation despite the failure of the wee parton limit used in earlier discussions of this connection [3, 4]. In Secs. IV C and IV D, our results are compared with other extensions of quark distributions to ultra small x based on conventional parton-level fits to the HERA data. We summarize and draw conclusions in Sec. V.

II. EXTRAPOLATION OF $F_2^{\gamma p}(x, Q^2)$ TO ULTRA SMALL x

As we emphasized in the Introduction, for the energies E_ν of interest for UHE neutrino cross sections, we must know $F_2^{\gamma p}(x, Q^2)$ at values of x many orders of magnitude below the range where it has been measured at HERA. To cover the highest energy range reached by neutrino telescope searches [14, 15], $E_\nu \sim 10^{17}$ GeV, requires an extrapolation of eight orders of magnitude in x below the lowest values $x \sim 10^{-5}$ – 10^{-6} encountered at HERA. While this is actually only a factor of ~ 3 increase in the maximum value of the natural variable $v \equiv \ln(1/x)$, it is still essential that the form used to extrapolate $F_2^{\gamma p}(x, Q^2)$ be consistent with both the asymptotic limiting behavior expected theoretically and the present data. If a fit to the data indicates that the measured structure function is already consistent with the limiting asymptotic form, the extrapolation may be expected to be robust; our approach, which we summarize here, has this feature. It is the best one can do.

Up to well understood corrections, the reduced cross section reported experimentally [17] is equal to $F_2^{\gamma p}(x, Q^2)$. This structure function contains all of the strong interaction dynamics, a point made clearly in Ref. [1]. From the point of view of vector dominance, expected to hold at high energies and large Q^2 [18], it is just the extension of real γp scattering with photon 4-momentum squared $q^2 = 0$, to virtual $\gamma^* p$ scattering with a virtual photon 4-momentum squared $q^2 = -Q^2 < 0$. We denote the Mandelstam variables for $\gamma^* p$ scattering by \hat{s} , \hat{t} , and \hat{u} .

There appears to be no obstacle to the continuation from $q^2 = 0$ to an off-shell $q^2 = -Q^2 < 0$. The total cross section for virtual photon-nucleon ($\gamma^* p$) scattering is proportional to the virtual forward Compton scattering amplitude for zero momentum transfer to the nucleon, $\hat{t} = (p - p')^2 = 0$. A complete all-orders analysis of the latter in perturbation theory [18] shows that it is real analytic in the Mandelstam variable $\hat{s} = (p + q)^2$ for the scattering of a virtual photon from a nucleon for $Q^2 > -m_\pi^2$, with the usual normal thresholds in \hat{s} and \hat{u} . Analyticity in \hat{t} can also be established for

$Q^2 > 0$ for the leading perturbative diagrams, and presumably holds in general. Given these results, the arguments of Martin [19–21] establish the Froissart bound [22] for the γ^*p cross section, hence $F_2^{\gamma p}$.

The phenomenological success of vector meson dominance of the electromagnetic current matrix elements between hadronic states provides physical evidence that the required off-shell continuation from photo-production to DIS electron-nucleon scattering is correct and relevant [23–25]. Furthermore, the continuations in mass-variables for on-shell pion to off-shell weak-currents in PCAC-current algebra relations have had a history of remarkably successful predictions [23, 24, 26].

Extensive analyses of experimental data on high energy hadronic and photo-production cross sections dramatically demonstrate the early appearance of the $\ln^2 \hat{s}$ Froissart-like behavior [5, 10, 11]. This can be understood in terms of QCD processes at the quark-gluon level [27–30]. Since deep inelastic γ^*p scattering is smoothly connected to γp scattering by continuation in Q^2 [18], it is natural to assume the $\ln^2 s$ Froissart behavior of the photo-production cross section will also appear in DIS for high γ^*p energies with the substitution $s \rightarrow \hat{s}$. In fact, detailed perturbative arguments [31] indicate that unitarity begins to be violated at remarkably small values of $v = \ln(1/x)$, e.g. for $v \gtrsim 3$ at $Q^2 = 10^4 \text{ GeV}^2$, in the usual description of the QCD evolution of $F_2^{\gamma p}$ through the Dokshitzer-Gribov-Lipitov-Altarelli-Parisi (DGLAP) equations [32–34], suggesting the onset of non-perturbative Froissart-like behavior.

The role of Mandelstam s is played in γ^*p scattering by $\hat{s} = W^2$, the final state hadronic energy squared:

$$\hat{s} \equiv W^2 = (q + p)^2 = \frac{Q^2}{x}(1 - x) + m^2 \rightarrow \frac{Q^2}{x}, \quad x \rightarrow 0. \quad (1)$$

For Q^2 fixed and large relative to the square of the nucleon mass, i.e., $Q^2 \gg m^2$, Eq. (1) shows that a saturated $\ln^2 \hat{s}$ bound on the γ^*p cross section translates into a $\ln^2(1/x) = v^2$ bound on the small x (large v) behavior of $F_2^{\gamma p}$.

In their analysis of the early ZEUS data on $F_2^{\gamma p}(x, Q^2)$ [35, 36], Berger, Block, and Tan [1] assumed that the γ^*p cross section should show Froissart-like behavior in $1/x$. The success of their model amply supports this assumption. In a subsequent paper [2], those authors refined their saturated “Froissart” parameterization and obtained an excellent global fit to both the x and Q^2 dependence of the ZEUS data, with 6 free parameters describing hundreds of points of data. This fit was later used along with the Feynman wee parton picture to predict the UHE ν - N cross sections [3].

Releasing one more parameter, the present authors [4, 16] fit the joint ZEUS [35, 36] and H1 [37] determinations of the $e^\pm p$ DIS cross sections as combined by those groups [17], a combination that resolved some of the tension between previous individual ZEUS and H1 analyses. This fit, summarized below, provides very accurate values of $F_2^{\gamma p}(x, Q^2)$ over a large region of the x - Q^2 plane that includes some 335 data points. It was used in [4] in conjunction with the wee parton picture to predict UHE neutrino cross sections for two full quark families based on the extrapolation of the analytic expression for $F_2^{\gamma p}$ into the $Q^2 > M_Z^2$ and $x < 10^{-10}$ regions needed to evaluate the cross sections up to $E_\nu = 10^{14} \text{ GeV}$ and beyond. In our companion paper, Part II, we improve this calculation by including the b-quark and the NLO corrections to the wee parton limit, and extend the energy range up to the $E_\nu = 10^{17} \text{ GeV}$ energy reported by several neutrino detectors [14, 15].

The global fit function used in [2] and [16], which ensures that the saturated Froissart $\ln^2(1/x)$ behavior dominates at small x , takes the form

$$\begin{aligned} F_2^{\gamma p}(x, Q^2) = & (1 - x) \left[\frac{F_P}{1 - x_P} + A(Q^2) \ln \left(\frac{x_P}{x} \frac{1 - x}{1 - x_P} \right) \right. \\ & \left. + B(Q^2) \ln^2 \left(\frac{x_P}{x} \frac{1 - x}{1 - x_P} \right) \right], \end{aligned} \quad (2)$$

where

$$\begin{aligned} A(Q^2) &= a_0 + a_1 \ln Q^2 + a_2 \ln^2 Q^2, \\ B(Q^2) &= b_0 + b_1 \ln Q^2 + b_2 \ln^2 Q^2. \end{aligned} \quad (3)$$

As is evident from Eq. (1), this form is equivalent to the quadratic expression in $\ln s$ familiar in fits to hadronic data [5], with the Q^2 dependence rearranged and extended.

At small x or large $v = \ln(1/x)$, the expression in Eq. (2) becomes a quadratic polynomial in v with

$$\hat{F}_2^{\gamma p}(v, Q^2) \equiv F_2^{\gamma p}(e^{-v}, Q^2) \rightarrow \hat{C}_{0f}(Q^2) + \hat{C}_{1f}(Q^2)v + \hat{C}_{2f}(Q^2)v^2 + O(e^{-v}). \quad (4)$$

The coefficients \hat{C}_i are again quadratics in $\ln Q^2$,

$$\hat{C}_{0f}(Q^2) = F_P/(1 - x_P) + A(Q^2)v_0 + B(Q^2)v_0^2, \quad (5)$$

$$\hat{C}_{1f}(Q^2) = A(Q^2) + 2B(Q^2)v_0, \quad (6)$$

$$\hat{C}_{2f}(Q^2) = B(Q^2), \quad (7)$$

where $v_0 = \ln[x_P/(1-x_P)]$. We will use this structure repeatedly in the analysis below. As we will see in the Appendix, the neglect of the terms of order e^{-v} in Eq. (4), important for $v \sim 0$, will not affect our results at large v .

The procedure used in fitting the combined HERA data is described in references [38] and [16]. The parameter x_P was fixed at the value 0.11; the HERA data are sparse for larger x . F_P , the value of $F_2^{\gamma p}$ at x_P , and the other 6 fitting parameters are listed in Table I together with their errors. Also shown are the renormalized minimized χ^2 value [38], the number of degrees of freedom and the renormalized χ^2 per degree of freedom for our new analytic form for the combined ZEUS and H1 results [17].

TABLE I: Results of a 7-parameter fit to the HERA combined data for $F_2^{\gamma p}(x, Q^2)$ for $0.85 \leq Q^2 \leq 3000 \text{ GeV}^2$ and $x \leq 0.1$. The χ_{\min}^2 is renormalized by the factor $\mathcal{R} = 1.1$ to take into account the effects of the cut at $\Delta\chi_{i,\max}^2 = 6$ introduced by the sieve algorithm used in the fit [38].

Parameters	Values
a_0	$-8.471 \times 10^{-2} \pm 2.62 \times 10^{-3}$
a_1	$4.190 \times 10^{-2} \pm 1.56 \times 10^{-3}$
a_2	$-3.976 \times 10^{-3} \pm 2.13 \times 10^{-4}$
b_0	$1.292 \times 10^{-2} \pm 3.62 \times 10^{-4}$
b_1	$2.473 \times 10^{-4} \pm 2.46 \times 10^{-4}$
b_2	$1.642 \times 10^{-3} \pm 5.52 \times 10^{-5}$
F_P	0.413 ± 0.003
χ_{\min}^2	352.8
$\mathcal{R} \times \chi_{\min}^2$	391.4
d.o.f.	335
$\mathcal{R} \times \chi_{\min}^2/\text{d.o.f.}$	1.17

The high quality of our Froissart-bounded fit to data that range at the limits over ~ 5 orders of magnitude in x and ~ 3 orders of magnitude in Q^2 lends strong support to the proposal that the cross section for nucleon scattering with off-shell photons obeys the saturated Froissart bound in the γ^*p Mandelstam variable $\hat{s} = W^2$. The errors in the parameters a_i and b_i are typically a few percent except for b_1 ; this is not well determined, with a size and error of the order of the errors in the other parameters. Since the fit depends linearly on the parameters, the errors propagate linearly, and the correlated percentage errors in the extrapolation of our fit to ultra-small x are quite small.

III. DERIVATION OF LOW- x QUARK DISTRIBUTIONS FROM $F_2^{\gamma p}$

A. Relations for the quark distributions

We start by introducing the non-singlet (NS) quark distributions [39]

$$V_i = x(q_i - \bar{q}_i), \quad i = 1, 2, \dots, \quad (8)$$

$$T_3 = x(u + \bar{u} - d - \bar{d}), \quad (9)$$

$$T_8 = x(u + \bar{u} + d + \bar{d} - 2s - 2\bar{s}), \quad (10)$$

$$T_{15} = x(u + \bar{u} + d + \bar{d} + s + \bar{s} - 3c - 3\bar{c}), \quad (11)$$

$$T_{24} = x(u + \bar{u} + d + \bar{d} + s + \bar{s} + c + \bar{c} - 4b - 4\bar{b}), \quad (12)$$

and the singlet distribution

$$F_s = x(u + \bar{u} + d + \bar{d} + s + \bar{s} + c + \bar{c} + b + \bar{b} + \dots), \quad (13)$$

where the quark distributions are all defined at a given order in perturbative QCD.

We will be concerned mainly with very small x . We will take $s = \bar{s}$, $c = \bar{c}$, and $b = \bar{b}$, and will neglect the small differences between the \bar{u} and \bar{d} quarks at large x . The effects of the valence quark distributions $u_v = V_1$ and $d_v = V_2$ are also quite small, and we will take $d_v = (1/2)u_v$, with $u_v \equiv U$, a reasonable approximation, while $T_3 \rightarrow (1/2)U$.

F_s is then related to the γ^*p structure function for different numbers n_f of active quarks as

$$F_s(x, Q^2) = \frac{9}{2}F_{20}^{\gamma p}(x, Q^2) - \frac{1}{4}T_8(x, Q^2) - \frac{3}{8}U(x, Q^2), \quad n_f = 3, \quad (14)$$

$$F_s(x, Q^2) = \frac{18}{5}F_{20}^{\gamma p}(x, Q^2) - \frac{1}{5}T_8(x, Q^2) + \frac{1}{5}T_{15}(x, Q^2) - \frac{3}{10}U(x, Q^2), \quad n_f = 4, \quad (15)$$

$$F_s(x, Q^2) = \frac{45}{11}F_{20}^{\gamma p}(x, Q^2) - \frac{5}{22}T_8(x, Q^2) + \frac{5}{22}T_{15}(x, Q^2) - \frac{3}{22}T_{24}(x, Q^2) - \frac{15}{44}U(x, Q^2), \quad n_f = 5. \quad (16)$$

Here $F_{20}^{\gamma p}$ is an expression of LO form in terms of the quark distributions,

$$F_{20}^{\gamma p} = \sum_{i=1}^{n_f} e_i^2 x(q_i + \bar{q}_i), \quad (17)$$

with the sum running over the active quarks. We will be concerned later with values of Q^2 above the b -quark excitation threshold at m_b^2 , but not so large that t -quark effects are significant, so will generally take $n_f = 5$ in the following discussion.

The measured structure function $F_2^{\gamma p}$ is related to $F_{20}^{\gamma p}$ by convolution with QCD corrections from the operator product expansion [40–42],

$$x^{-1}F_2^{\gamma p} = \left[\mathbb{1} + \frac{\alpha_s}{2\pi}C_{2q} \right] \otimes (x^{-1}F_{2,0}^{\gamma p}) + \frac{\alpha_s}{2\pi} \left(\sum_i e_i^2 \right) C_{2g} \otimes g, \quad (18)$$

where $\mathbb{1}$ is the unit operator and the convolution \otimes is defined in Eq. (A.2). The coefficient functions C_{2q} and C_{2g} are given in [39] to NLO. Conversely,

$$x^{-1}F_{20}^{\gamma p} = \left[\mathbb{1} + \frac{\alpha_s}{2\pi}C_{2q} \right]^{-1} \otimes \left(x^{-1}F_2^{\gamma p} - \frac{\alpha_s}{2\pi} \left(\sum_i e_i^2 \right) C_{2g} \otimes g \right). \quad (19)$$

The inverse operator can be evaluated using Laplace transforms as discussed in the Appendix. This requires an input for the gluon distribution $g(x, Q^2)$. We take this from existing analyses of DIS data which give the gluon distribution in the HERA region, extending the fits to large v using quadratic extrapolations, a form implied by the DGLAP evolution equations [32–34] for an input F_s quadratic in v [16, 43, 44]. We will assume that $F_{20}^{\gamma p}$ is known.

It is useful to note that T_{15} and T_{24} are given directly at $Q^2 = m_c^2, m_b^2$, the thresholds for c and b production where the c and b distributions vanish, by the F_s distributions for $n_f = 3$ and 4 at those thresholds,

$$T_{15}(x, m_c^2) = F_s(x, m_c^2), \quad T_{24}(x, m_b^2) = F_s(x, m_b^2). \quad (20)$$

In particular, the x dependence of the T_{15} and T_{24} is determined at the thresholds.

We can use the expressions above to solve for the s, c, b , and light-quark distribution functions at small x where we can ignore valence effects and the very small splittings between the u and d distributions generated by V_1, V_2 , and T_3 and set those functions equal to zero. Then with xq_ℓ denoting the common small- x distribution function $\bar{u} = \bar{d}$ and with $\bar{s} = s, \bar{c} = c$, and $\bar{b} = b$, the quark distributions for $n_f = 5$ are

$$xs = xq_\ell - \frac{1}{4}T_8, \quad (21)$$

$$xc = xq_\ell - \frac{1}{12}T_8 - \frac{1}{6}T_{15}, \quad (22)$$

$$xb = xq_\ell - \frac{1}{12}T_8 - \frac{1}{24}T_{15} - \frac{1}{8}T_{24}; \quad (23)$$

$$xq_\ell = \frac{1}{10} \left(F_s + \frac{5}{6}T_8 + \frac{5}{12}T_{15} + \frac{1}{4}T_{24} - \frac{15}{4}U \right). \quad (24)$$

We want to use these expressions to investigate the behavior of the quark distributions at ultra-low x and large Q^2 implied by our Froissart-bounded model for $F_2^{\gamma p}$. This requires that we know $G(x, Q^2) = xg(x, Q^2)$ for use in Eq. (19), as well as $U(x, Q^2), T_8(x, Q^2), T_{15}(x, Q^2)$, and $T_{24}(x, Q^2)$. We will take $U(x, Q^2)$ and $T_8(x, Q^2)$ from existing parton-level fits to the HERA data, with $T_8(x, Q^2)$ extrapolated to small x using quadratic expressions in $v = \ln(1/x)$.

With this input, we can determine $F_{20}^{\gamma p}(x, Q^2)$ from our fit to the HERA data using Eq. (19), and $F_s(x, Q^2)$ for $n_f = 3, Q^2 \leq m_c^2$ from Eq. (14). The latter, evaluated at $Q^2 = m_c^2$, determines $T_{15}(x, m_c^2)$ through Eq. (20). We

can then calculate the evolution of $T_{15}(x, Q^2)$ to $Q^2 = m_b^2$ using the results in [45], and then repeat the process to obtain T_{24} . We will show before proceeding that the effects of non-singlet QCD evolution are small so that $T_{15}(x, Q^2) \approx T_{15}(x, m_c^2)$ and $T_{24}(x, Q^2) \approx T_{24}(x, m_b^2)$, and will derive approximate analytic expressions for the evolved functions. We use the latter in our numerical calculations.. We return to the discussion of the quark distributions in Sec. IV A.

B. Non-singlet evolution

Any of the non-singlet distributions evolves in Q^2 according to the equation [45]

$$\hat{F}_{NS}(v, Q^2) = \int_0^v dw K_{NS}(w, Q^2) \hat{F}_{NS}(v - w, Q_0^2), \quad (25)$$

where $v = \ln(1/x)$, $\hat{F}_{NS}(v, Q^2) = F_{NS}(e^{-v}, Q^2)$, and K_{NS} is the evolution kernel

$$K_{NS}(v, Q^2) = \frac{1}{2\pi i} \int_{-i\infty+\epsilon}^{i\infty+\epsilon} ds e^{vs} k_{NS}(s, Q^2), \quad (26)$$

$$k_{NS}(s, Q^2) = \exp \left[\sum_n \tau_n \Phi_{NS}^{(n)}(s) \right]. \quad (27)$$

Here $\Phi_{NS}^{(n)}$ is the Laplace transform with respect to v of the n^{th} order non-singlet splitting function in x , and

$$\tau_n(Q^2, Q_0^2) = \left(\frac{1}{4\pi} \right)^n \int_{Q_0^2}^{Q^2} d(\ln Q'^2) \alpha_s^n(Q'^2). \quad (28)$$

In leading order ($n = 1$), $\Phi_{NS}^{(1)}$ is just Φ_f as defined in [46], and can be written as

$$\Phi_{NS}^{(1)}(s) = \frac{4}{3} \left(\frac{2s}{s+1} + \frac{s}{s+2} \right) - \frac{16}{3} [\psi(s+1) - \psi(1)], \quad (29)$$

where $\psi(z) = \Gamma'(z)/\Gamma(z)$ is the digamma function. The function $\Phi_{NS}^{(1)}(s)$ clearly vanishes at $s = 0$. Its only singularities in the complex s plane are poles at $s = -1, -2, \dots$, with the rightmost singularity at $s = -1$ (where here s denotes a variable in Laplace space and is *not* the Mandelstam invariant). We can therefore move the contour of integration in Eq. (26) to a line parallel to the imaginary axis with the real part of s to the left of $s = 0$, but still to the right of $s = -1$, without encountering any singularities.

The integrand diverges for $s \rightarrow -1$ and $s \rightarrow \infty$, and has its minimum value on the real axis at the point $s_0 \approx -1 + \sqrt{8\tau_1/3v_1}$ near -1 where the derivative of the exponent with respect to s vanishes. Here v_1 is given by $v_1 \approx v - (8/9)(\pi^2 - 3)\tau_1$, so $v_1 \rightarrow v$ for v large. The integrand has a value proportional to $\exp[vs_0 + \tau_1 \Phi_{NS}^{(1)}(s_0)] \approx \exp[-v + \sqrt{32\tau_1 v_1/3} + O(1/v_1)]$ at this saddle point. If we take the line of integration to run through the saddle point, we can estimate the integral using the method of steepest descents; the result is proportional to $\exp[-v + \sqrt{32\tau_1 v_1/3}]$.

Given the behavior of the integrand, we see that the integral is exponentially suppressed for $v \gg 32\tau_1/3$. As a result, the kernel $K_{NS}^{(1)}$ is effectively zero except in a region in v extending only a distance $\sim 32\tau_1/3$ from $v = 0$. This is small relative to v for the values of Q^2 and v of primary interest here. For example, $\tau_1 = 0.108$ for $Q^2 = 10^4 \text{ GeV}^2$, so the constraint requires only that $v \gg 1.2$ or $x \ll 0.3$. However, $v > 11.5$ for $x < 10^{-5}$, the region of primary interest, so the integral in Eq. (25) samples only values of $\hat{F}_{NS}(v - w)$ very near v .

To exploit this observation, we replace w by zero in the factor $\hat{F}_{NS}(v - w, Q_0^2)$ in Eq. (25) and shift the contour in Eq. (27) to the left of $s = 0$. We find that

$$\begin{aligned} \hat{F}_{NS}(v, Q^2) &\approx \hat{F}_{NS}(v, Q_0^2) \int_0^v dw K_{NS}(w, Q^2) \\ &= \hat{F}_{NS}(v, Q_0^2) \int_0^v dw \frac{1}{2\pi i} \int_{-i\infty-c}^{i\infty-c} ds e^{ws} k_{NS}(s, Q^2) \\ &= \hat{F}_{NS}(v, Q_0^2) \frac{1}{2\pi i} \int_{-i\infty-c}^{i\infty-c} ds \frac{1}{s} (e^{vs} - 1) e^{\tau_1 \Phi_{NS}^{(1)}(s)}. \end{aligned} \quad (30)$$

Since $\text{Re } s < 0$, the first term in the integrand is exponentially small for v large and positive and can be dropped. We can close the contour to the right in the remaining term, and find that, for $v \gg 32\tau_1/3$ and $v \gg 1$,

$$\hat{F}_{NS}^{(1)}(v, Q^2) \approx \hat{F}_{NS}(v, Q_0^2) e^{\tau_1 \Phi_{NS}^{(1)}(0)} = \hat{F}_{NS}(v, Q_0^2) \quad (31)$$

where the last relation uses the fact that $\Phi_{NS}^{(1)}(0) = 0$. That is, *there is essentially no change in the NS distribution $\hat{F}_{NS}(v, Q_0^2)$ under LO evolution.*

This result generalizes to higher orders: $\Phi_{NS}^{(n)}(s)$ has no singularities in s to the right of $s = -1$ in NLO and NNLO, and presumably also higher orders, and $\Phi_{NS}^{(n)}(0) = 0$ for all n , so, following the argument above, $\hat{F}_{NS}(v, Q^2) \approx \hat{F}_{NS}(v, Q_0^2)$ for v sufficiently large.

The large- v part of the argument is essentially unchanged. To see that $\Phi_{NS}^{(n)}(0) = 0$, we note that $\Phi_{NS}^{(n)}(s)$ is just the Laplace transform of the n^{th} order quark splitting function,

$$\Phi_{NS}^{(n)}(s) = \int_0^\infty dw e^{-w(s+1)} \hat{P}^-(w) = \int_0^\infty dw e^{-w(s+1)} \left(\hat{P}_{qq}(w) - \hat{P}_{q\bar{q}}(w) \right), \quad (32)$$

where we follow the notation in [39] with the substitution of e^{-w} for x and $\hat{P}^-(w) = P^-(e^{-w})$. For $s = 0$, this reduces to

$$\begin{aligned} \Phi_{NS}^{(n)}(0) &= \int_0^\infty dw e^{-w} \left(\hat{P}_{qq}(w) - \hat{P}_{q\bar{q}}(w) \right) \\ &= \int_0^1 dx \left(P_{qq}(x) - P_{q\bar{q}}(x) \right) = 0. \end{aligned} \quad (33)$$

This expression vanishes as the result of quark number conservation [39]. The insensitivity of any NS distribution $\hat{F}_{NS}(v, Q^2)$ to QCD evolution follows. We conclude that the result in Eq. (31) continues to hold, with negligible corrections because of the smallness of the higher-order parameters τ_n in Eq. (27), $\tau_n \ll \tau_1$, $n > 1$.

To see what residual effects there are in a realistic case, suppose that $\hat{F}_{NS}(v, Q_0^2) = \sum_{n=0}^2 c_n v^n$; this is the asymptotic form of our Froissart-bounded fit to the HERA data, Eq. (4) at large v , and is also the form of any of the non-singlet distributions listed above. It is useful in this case to use the alternative form of Eq. (25) given by the convolution theorem for Laplace transforms,

$$\hat{F}_{NS}(v, Q^2) = \mathcal{L}^{-1} [k_{NS}(s, Q_0^2) f_{NS,0}(s); v], \quad (34)$$

where $f_{NS,0}(s)$ is the Laplace transform of the initial distribution $\hat{F}_{NS}(v, Q_0^2)$ at Q_0^2 with respect to v , $f_{NS,0}(s) = \sum_{n=0}^2 c_n n! / s^{n+1}$. In LO, this gives the evolved function

$$\hat{F}_{NS}(v, Q^2) = \sum_{n=0}^2 c_n \frac{n!}{2\pi i} \int_{-i\infty+\epsilon}^{i\infty+\epsilon} \frac{ds}{s^{n+1}} e^{vs+\tau_1(Q^2, Q_0^2) \Phi_{NS}^{(1)}(s)}. \quad (35)$$

Since the only singularity of the integrand to the right of $s = -1$ is the pole $1/s^{n+1}$ at $s = 0$, we can shift the integration contour to the left of $s = 0$ as shown in Fig. 1, picking up the residue of the function $\exp[vs + \tau_1 \Phi_{NS}^{(1)}(s)]$ at the pole, and find that

$$v^n \rightarrow \left. \frac{d^n}{ds^n} e^{vs+\tau_1 \Phi_{NS}^{(1)}(s)} \right|_{s=0} + \frac{n!}{2\pi i} \int_{-i\infty-c}^{i\infty-c} \frac{ds}{s^{n+1}} e^{vs+\tau_1 \Phi_{NS}^{(1)}(s)}. \quad (36)$$

The line integral which remains can be taken to run through the slightly-shifted saddle point near $s = -1$, and again gives a contribution which is exponentially small for v large and can be dropped.

For an input distribution v^2 , we get an evolved distribution

$$v^2 \rightarrow \left[v - \left(\frac{8\pi^2}{9} - \frac{10}{3} \right) \tau_1 \right]^2 - \left(6 + \frac{16}{3} \psi''(1) \right) \tau_1 + O(e^{-v}) \quad (37)$$

$$= (v - 5.4397\tau_1)^2 + 6.8219\tau_1. \quad (38)$$

Similarly,

$$v \rightarrow v - \left(\frac{8\pi^2}{9} - \frac{10}{3} \right) \tau_1 + O(e^{-v}) = v - 5.4397\tau_1. \quad (39)$$

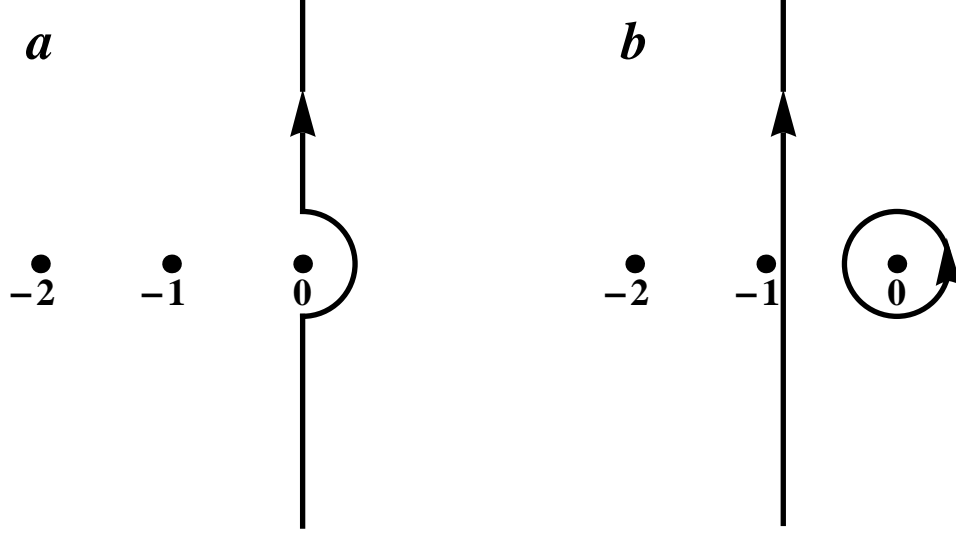


FIG. 1: Integration contours for the inverse Laplace transforms in Eq. (35) and Eq. (A.28): (a), the original contour $(-i\infty + \epsilon, i\infty + \epsilon)$ which avoids the rightmost poles of the integrands at $s = 0$ on the right; (b), the shifted contour, broken into a loop around the origin in the s plane, and a line integral just to the right of the singularity at $s = -1$. That integral can be taken most efficiently to run through the saddle point near -1 . There are further singularities at $s = -2, \dots$, indicated by dots.

Finally, since $\Phi_{NS}^{(1)}(0) = 0$, a constant input function is unchanged in the evolution up to exponentially small terms.

Combining terms and expressing the result in terms of $\hat{F}_{NS}(v, Q_0^2)$, Eq. (35) gives the evolved distribution

$$\hat{F}_{NS}(v, Q^2) = \hat{F}_{NS}(v', Q_0^2) - c_2 \left(6 + \frac{16}{3} \psi''(1) \right) \tau_1(Q^2, Q_0^2) + O(e^{-v}), \quad (40)$$

$$v' = v - \left(\frac{8\pi^2}{9} - \frac{10}{3} \right) \tau_1(Q^2, Q_0^2), \quad (41)$$

where $c_2 \equiv \hat{C}_{2,NS}(Q_0^2)$ is the coefficient of v^2 in $\hat{F}_{NS}(v, Q_0^2)$. The NS evolution has simply shifted v by a small τ_1 -dependent constant and added a small constant term. For example, $v \rightarrow v' = v - 0.587$ with an additive constant $0.736 c_2$ for $Q^2 = 10^4 \text{ GeV}^2$, $Q_0^2 = 4.5 \text{ GeV}^2$, $\tau_1 = 0.108$. The constant term can be neglected for the values of v of primary interest here. We find, therefore, that an excellent approximation for the complete evolved distribution is $\hat{F}_{NS}(v, Q^2) = \hat{F}_{NS}(v', Q_0^2)$.

IV. QUARK DISTRIBUTIONS AT VERY SMALL x

A. Results

We will only look at the quark distributions in the region of large Q^2 , so will take $n_f = 5$. Then from Eq. (16) with $T_3 = 0$, F_s is given in v space by

$$\hat{F}_s = \frac{45}{11} \hat{F}_{20}^{\gamma p} - \frac{5}{22} \hat{T}_8 + \frac{5}{22} \hat{T}_{15} - \frac{3}{22} \hat{T}_{24} - \frac{15}{44} \hat{U}, \quad n_f = 5, \quad (42)$$

where \hat{T}_i and \hat{U} are T_i and U evaluated in v space, with $x \rightarrow e^{-v}$.

We have determined $\hat{F}_{20}^{\gamma p}$ from $\hat{F}_2^{\gamma p}$ using the NLO transformation in Eq. (19) as described in the Appendix. The results are given analytically for large v in Eq. (A.31). We used a gluon distribution \hat{G} obtained from a fit to the CT10 gluon distribution [47, 48] of the form in Eq. (4), quadratic in v and $\ln Q^2$. This form is necessary for consistency of the DGLAP evolution equations if $\hat{F}_2(v, Q^2)$ has this form. The expression for \hat{G} was fitted over the region $2 \times 10^{-4} \leq x \leq 0.01$ and $10 \text{ GeV}^2 \leq Q^2 \leq 1000 \text{ GeV}^2$, and then extended to all v, Q^2 . We note that the CT10 gluon distributions obtained in NLO and NNLO are very similar, and agree also with the HERAPDF results [17, 48]. The resulting $\hat{F}_{20}^{\gamma p}$, with the transformation in Eq. (19) calculated in NLO, is compared with $\hat{F}_2^{\gamma p}$ in Fig. 2. The changes

are on the order of 5-10%, with a much smaller uncertainty from the gluon term. While we regard it as unlikely that higher order contributions to the functions C_{2q} and C_{2g} in Eq. (19) would affect the results for $\hat{F}_{20}^{\gamma p}$ significantly, we emphasize that any effects would be in the individual quark distributions, and would be insignificant for the relations between $\hat{F}_2^{\gamma p}$ and the corresponding structure functions $\hat{F}_2^{\nu(\bar{\nu})}$ and $\hat{F}_0^{\nu(\bar{\nu})}$ for charged- and neutral-currents neutrino-nucleon scattering given in Eqs. (47) and (51) because of the smallness of the \hat{T}' terms in those equations.

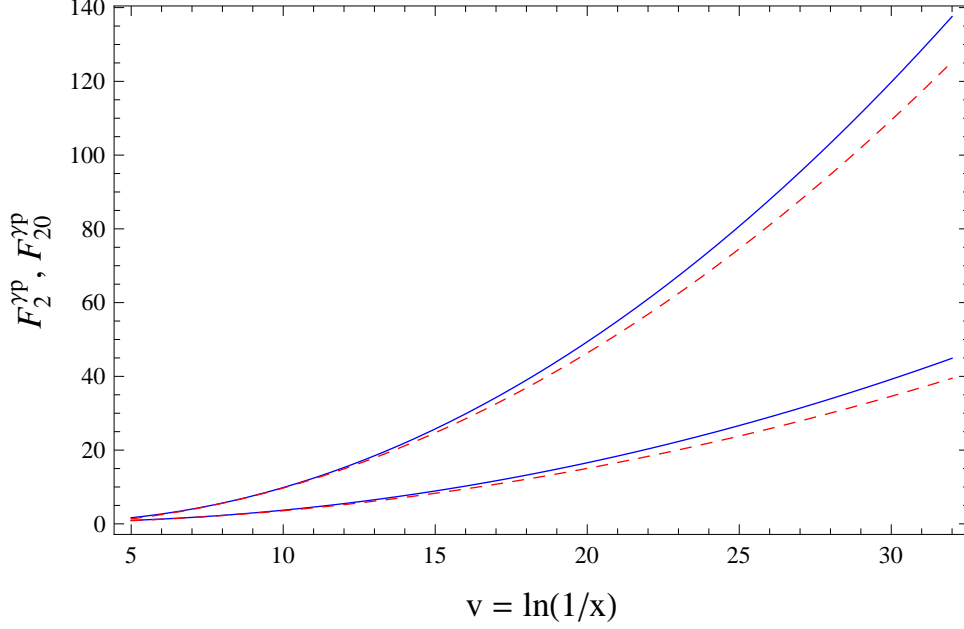


FIG. 2: Comparison of the quark-level distribution $\hat{F}_{20}^{\gamma p}$ in v space (red dashed curves) with the large- v extension of our Froissart form fit to the HERA data, Eq. (4) (solid blue curves), for $Q^2 = 10^4$ GeV² (top curves) and $Q^2 = 100$ GeV² (bottom). The two are related by Eq. (19) as implemented in the Appendix through the relation in Eq. (A.31).

To get an approximate extension of the (small) function \hat{T}_8 to small x or large v , we use a quadratic fit to \hat{T}_8 as a function of v as determined from the CT10 PDFs [47, 48] over the region $10^{-5} < x < 0.003$ for $Q^2 = m_c^2$, and calculate it for larger Q^2 using the expression in Eq. (40). We then determine \hat{T}_{15} and \hat{T}_{24} at the c and b thresholds $Q^2 = m_c^2, m_b^2$ using the expressions in Eq. (20), again evolved to higher Q^2 using Eq. (40). The relations in Eqs. (21) to (24) then determine the s, c, b , and light quark distributions in terms of $\hat{F}_{20}^{\gamma p}$. The results are shown in Fig. 3 for $5 \leq v \leq 32.2$, corresponding to $0.0067 \geq x \geq 1 \times 10^{-14}$. For comparison, the lower limit of the HERA data is on the order of $x = 10^{-4}$, $v = 9.2$ for Q^2 of a few GeV².

B. Neutrino structure functions and the wee parton limit

The assumption that the differences between the quark distributions tend toward zero for small x and large Q^2 —the wee parton picture—was used in [3, 4] to calculate the neutrino and antineutrino cross sections on an isoscalar nucleon $N = (p + n)/2$ at very high energies in terms of $F_2^{\gamma p}$ as extrapolated to small x . We find here that there is not a proper wee parton limit. This may be seen from Fig. 4. The c and b distributions remain quite different from the light quark distribution at small x or large v and large Q^2 , with the c/q_ℓ and b/q_ℓ ratios implied by Eqs. (22)-(24) approaching nearly constant values at small x which decrease only logarithmically in Q^2 .

Perhaps surprisingly, this result does not affect the supposed “wee parton” calculation of the neutrino cross sections in practice. The dominant structure function in charged-current neutrino scattering is $F_2^{\nu(\bar{\nu})}$ is given in terms of quark distributions for $n_f = 5$ by

$$F_{20}^{\nu} = x(u + d + 2s + 2b + \bar{u} + \bar{d} + 2\bar{c}) \quad (43)$$

$$= F_s \quad (44)$$

$$= \frac{45}{11} F_{20}^{\gamma p} - \frac{1}{22} (5T_8 - 5T_{15} + 3T_{24}) - \frac{15}{44} U. \quad (45)$$

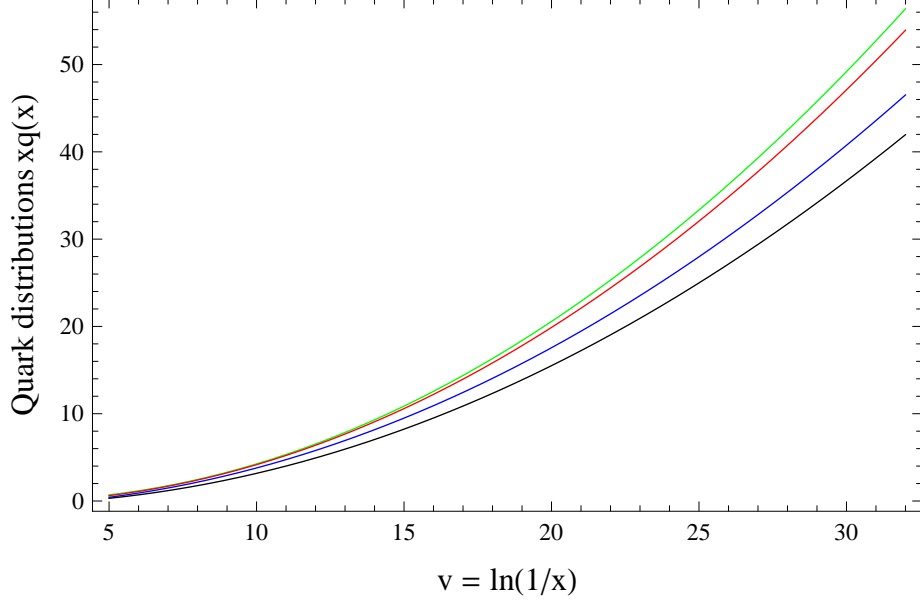


FIG. 3: Plots of quark distributions determined from the Froissart-bounded fit to $F_2^{\gamma p}$ versus $v = \ln(1/x)$ for $Q^2 = 10^4 \text{ GeV}^2$: top to bottom, $xq_\ell(x, Q^2)$ (green curve), $xs(x, Q^2)$ (red curve), $xc(x, Q^2)$ (blue curve), and $xb(x, Q^2)$ (black curve).

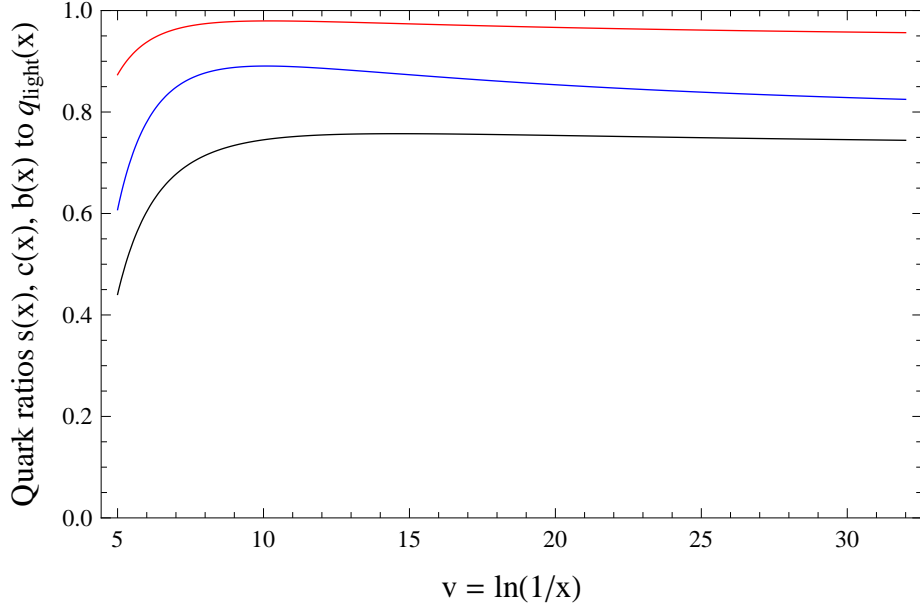


FIG. 4: The ratios, top to bottom, of the distributions xs/xq_ℓ (red curve), xc/xq_ℓ (blue curve), and xb/xq_ℓ (black curve) plotted versus $v = \ln(1/x)$ for $Q^2 = 10^4 \text{ GeV}^2$.

The results for antineutrino scattering are identical, $F_2^{\bar{\nu}} = F_2^{\nu}$.

We obtain the observable neutrino structure function $F_2^{\nu(\bar{\nu})}$ by applying the QCD corrections from the operator product expansion [39–42] to $F_{20}^{\nu(\bar{\nu})}$

$$x^{-1}F_2^{\nu(\bar{\nu})} = \left[\mathbb{1} + \frac{\alpha_s}{2\pi} C_{2q} \right] \otimes \left(x^{-1}F_{2,0}^{\nu(\bar{\nu})} \right) + \frac{\alpha_s}{2\pi} \left(\sum_i c_{2,i} \right) C_{2g} \otimes g, \quad (46)$$

where the coefficient functions C_{2q} and C_{2g} are given in Eq. (A.3) and Eq. (A.4), and the effective charges $c_{2,i}$ are the

coefficients of the quark distributions in Eq. (43). This transformation converts the $F_{20}^{\gamma p}$ term in Eq. (45) to $F_2^{\gamma p}$ as in Eq. (18). The gluon term in Eq. (46) is absorbed in the process, and only C_{2q} acts on the T_j in Eq. (45). The result in v space for $Q^2 > m_b^2$, $n_f = 5$, is

$$\hat{F}_2^{\nu(\bar{\nu})} = (45/11)\hat{F}_2^{\gamma p} - \frac{1}{22} \left(5\hat{T}'_8 - 5\hat{T}'_{15} + 3\hat{T}'_{24} \right) - \frac{15}{44}\hat{U}'. \quad (47)$$

The original functions $\hat{T}_i(v, Q^2)$ in v space are quadratic polynomials in v . The transformed functions $\hat{T}'_i(v, Q^2)$ are again quadratics for v large. Their calculation is discussed in the Appendix, where we show that up to a small additive constant $\hat{T}'(v, Q^2)$ is simply \hat{T} evaluated at a shifted value of v ,

$$\hat{T}'(v, Q^2) = \hat{T}(v_T, Q^2) + \text{constant} + \mathcal{O}(e^{-v}), \quad v_T = v + \text{constant}. \quad (48)$$

The details are given in the Appendix around Eq. (A.33).

In the wee parton limit $u = \bar{u} = d = \bar{d} = s = c = b = q_\ell$, the functions T'_i and U' in Eq. (47) vanish, and $F_{2,wee}^{\nu(\bar{\nu})} = (45/11)F_2^{\gamma p}$. The factor $45/11 = 10/(22/9)$ in this expression is just the ratio of the charge factors $(\sum_i c_{2,i})/(\sum_i e_i^2)$ for $n_f = 5$, a relation used in the case $n_f = 4$ in the calculations of neutrino cross section in [3, 4]. As seen in Fig. 5, the results for $\hat{F}_2^{\nu(\bar{\nu})}$ obtained in this limit agree very well for large v with those calculated using Eq. (47), for example, to $\sim 3.2\%$ (1.2%) at $v = 12$ (32) and $Q^2 = 100 \text{ GeV}^2$, with the errors decreasing with increasing Q^2 to 1.1% (0.4%) at $v = 12$ (32) for $Q^2 = 10,000 \text{ GeV}^2$, even though the wee limit does not really exist for the quark distributions derived here. These differences are just discernible in Fig. 5, and are not significant for applications at very small x or large v .

It is not obvious that the relation $F_2^{\nu(\bar{\nu})} \approx F_{2,wee}^{\nu(\bar{\nu})} = (45/11)F_2^{\gamma p}$ should hold as well as it does. In particular, the results in Fig. 4 show that the c and b PDFs are significantly smaller at all v than the light-quark PDF q_ℓ , while the valence distribution $U = u_v \approx 2d_v$ vanishes at large v . However, $F_2^{\gamma p}$ is fixed by experiment. The overall decrease in the contributions of the s , c and b quarks to $F_2^{\gamma p}$ is therefore compensated by an increase in q_ℓ . The c quark also appears with 4 times the weight of the s and b quarks in $F_2^{\gamma p}$, but equal weight in $\hat{F}_2^{\nu(\bar{\nu})}$, with the result that the different errors in $s + b$ and c tend to cancel in the latter; somewhat accidentally, the cancellation is nearly complete.

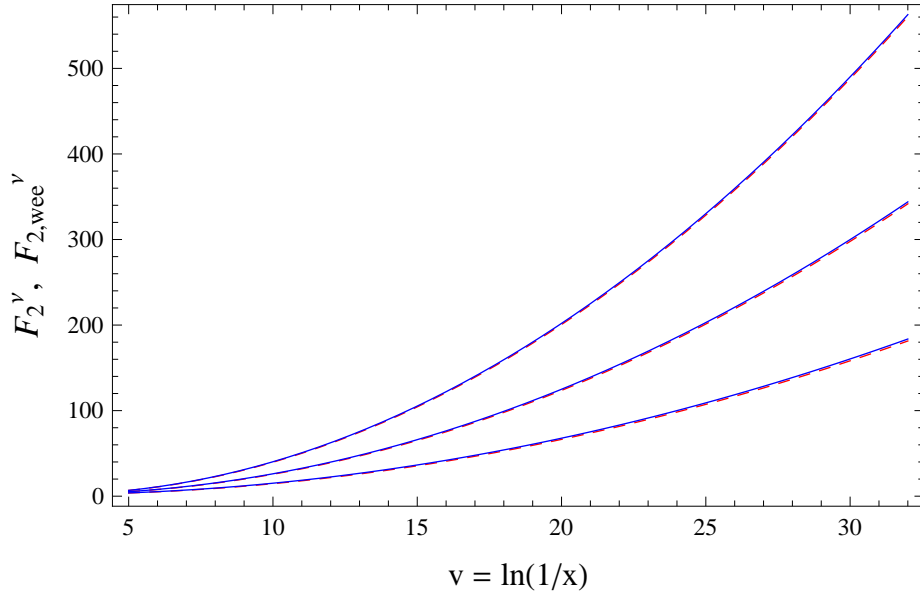


FIG. 5: Comparison of the dominant structure function $F_2^{\nu(\bar{\nu})}$ in charged current ν - N or $\bar{\nu}$ - N scattering calculated for, top to bottom, $Q^2 = 10,000, 1000$, and 100 GeV^2 using the complete expression in Eq. (47) (dashed red curves), and the approximate distributions $F_{2,wee}^{\nu} \approx (45/11)F_2^{\gamma p}$ (solid blue curves) derived assuming the validity of the wee parton limit for the quark distributions. The limits $v = 5$ (32) of the range shown correspond to $x = 0.007$ (10^{-14}).

Similar results hold for the structure functions for neutral current ν - N and $\bar{\nu}$ - N scattering. As discussed in the accompanying paper, Paper II, the dominant structure function is $F_2^{\nu(\bar{\nu})}$. The uncorrected function is given in terms

of the quark distributions by

$$F0_{20}^{\nu(\bar{\nu})} = x(d+u+\bar{d}+\bar{u})(L_u^2+R_u^2+L_d^2+R_d^2)/4 \\ + x(s+b+\bar{s}+\bar{b})(L_d^2+R_d^2)/2 + x(c+\bar{c})(L_u^2+R_u^2)/2 \quad (49)$$

$$= \frac{9}{22} \left(F_{20}^{\gamma p} - \frac{1}{12} U \right) [3(L_d^2+R_d^2) + 2(L_u^2+R_u^2)] \\ - \frac{1}{132} [4(L_d^2+R_d^2) - L_u^2 - R_u^2] (5T_8 - 5T_{15} + 3T_{24}). \quad (50)$$

The neutral current coefficients are $L_u = 1 - \frac{4}{3} \sin^2 \theta_W$, $L_d = -1 + \frac{2}{3} \sin^2 \theta_W$, $R_u = -\frac{4}{3} \sin^2 \theta_W$ and $R_d = \frac{2}{3} \sin^2 \theta_W$. We use the value $\sin^2 \theta_W = 0.231$ [49, 50] in all calculations.

Upon transforming to the physical structure function through Eq. (46), $F_{20}^{\gamma p} \rightarrow F_2^{\gamma p}$ and $T_i \rightarrow T'_i$ as above. The result in v space for $Q^2 > m_b^2$, $n_f = 5$ is

$$\hat{F}0_2^{\nu(\bar{\nu})} = \frac{9}{22} \left(\hat{F}_2^{\gamma p} - \frac{1}{12} \hat{U}' \right) [3(L_d^2+R_d^2) + 2(L_u^2+R_u^2)] \\ - \frac{1}{132} [4(L_d^2+R_d^2) - L_u^2 - R_u^2] (5\hat{T}'_8 - 5\hat{T}'_{15} + 3\hat{T}'_{24}). \quad (51)$$

The naive wee parton limit, with all quark and antiquark distributions assumed to be equal, $q_i \equiv \bar{q}_i \equiv q$, is obtained by taking the \hat{T}'_i and \hat{U}' as zero, giving $\hat{F}0_{2,wee}^{\nu(\bar{\nu})} = (9/22) \hat{F}_2^{\gamma p} \times [3(L_d^2+R_d^2) + 2(L_u^2+R_u^2)]$. The coefficient of $\hat{F}_2^{\gamma p}$ is just a ratio of the sums of charge factors $(\sum_i c_{2,i})/(\sum_i e_i^2)$ in Eqs. (49) and (17).

The exact results for $F0_2^{\nu(\bar{\nu})}$ in v space are compared to the wee approximation in Fig. 6. The agreement is very good for v large, with agreement to $\sim 3.8\%$ (1.5%) at $v = 12$, (32) for $Q^2 = 100 \text{ GeV}^2$, decreasing with increasing Q^2 to 1.3% (0.5%) at $v = 12$ (32) for $Q^2 = 10,000 \text{ GeV}^2$, even though, again, the wee limit does not really exist for the quark distributions derived here. These differences are quite small as seen in Fig. 6, and are not significant for applications to ultra high energy neutrino cross sections.

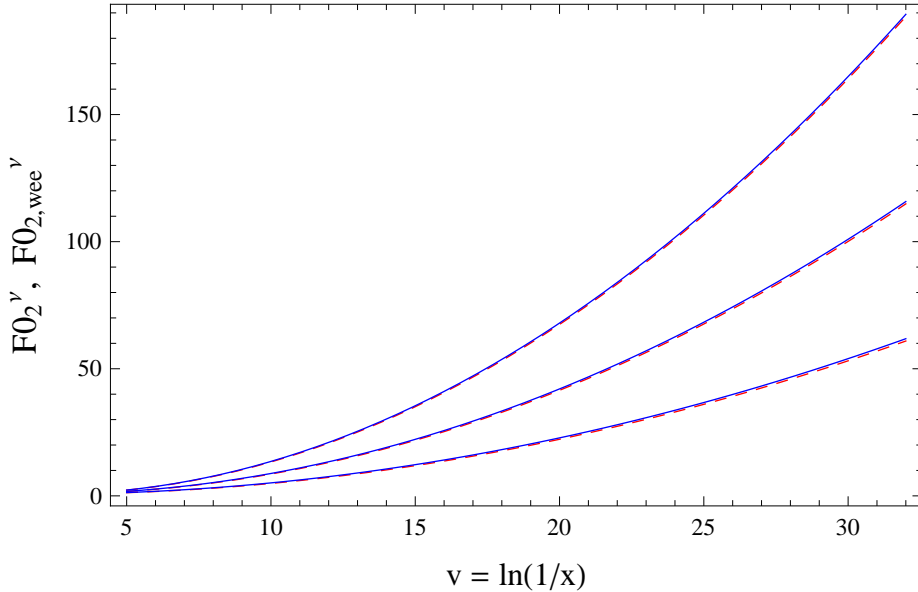


FIG. 6: Comparison of the dominant structure function $F0_2^{\nu(\bar{\nu})}$ in neutral current ν - N or $\bar{\nu}$ - N scattering calculated for, top to bottom, $Q^2 = 10,000, 1000$, and 100 GeV^2 using the complete expression in Eq. (51) (dashed red curves), and the approximate distributions $F0_{2,wee}^{\nu(\bar{\nu})} \approx (9/22) F_2^{\gamma p} [3(L_d^2+R_d^2) + 2(L_u^2+R_u^2)]$ (solid blue curves) derived assuming the validity of the wee parton limit for the quark distributions. The limits $v = 5$ (32) of the range shown correspond to $x = 0.007$ (10^{-14}).

To summarize, we have shown that the quark distributions derived from our Froissart-bounded fit to the HERA data do not satisfy the wee parton assumption, that all quark and antiquark distributions approach a common

limiting distribution at small x and large Q^2 . The quark distributions actually diverge from each other proportional to $v^2 = \ln^2(1/x)$ for v large. The dominant neutrino structure functions $F_2^{\nu(\bar{\nu})}$ and $F_0^{\nu(\bar{\nu})}$ calculated in terms of the quark distributions are nevertheless given to high fractional accuracy by the “wee parton” relations $F_2^{\nu(\bar{\nu})} \approx (\sum_i c_{2,i})/(\sum_i e_i^2) F_2^{\gamma p}$. This is important: $F_2^{\gamma p}$ is determined directly by data, and can be extrapolated to large v using a global fit to the v and Q^2 dependence of the data independently of the individual quark distributions. Our full results for UHE neutrino cross sections are discussed in detail in the accompanying paper [13].

C. Check of the wee parton limit in leading order

In this section, we compare the results above with those obtained at ultra-small x in a conventional approach based on the solution of the DGLAP evolution equations [32–34] starting from input boundary functions at a fixed initial value of Q^2 . Our main intent is to investigate the wee parton limit from a different point of view. We first consider a LO calculation based on boundary functions derived directly from our Froissart bounded fit to the HERA data *modulo* small non-singlet terms taken from earlier analyses by the CTEQ and MSTW groups. Our approach follows [16], using highly accurate and fast numerical algorithms for directly calculating inverse Laplace transforms [51–53], now modified to probe ultra-small x [54]. In particular, we can now calculate the Q^2 evolution of both singlet and non-singlet structure distributions down to x values as small as 10^{-14} , far below the range of the HERA data, and determine the quark distributions needed for the calculation of neutrino cross sections at neutrino energies up to $E_\nu = 10^{17}$ GeV.

We emphasize that our intent here is only to investigate the wee parton limit. A leading-order calculation is certainly not reliable at the very small x and large Q^2 needed for neutrino cross sections since higher order contributions in the QCD coupling α_s are known to be significant, and LO results also show systematic deviations from the HERA data [16]. However, if the wee parton limit fails at LO, it most likely fails at all orders.

The essential ingredients for a solution of the singlet DGLAP equations using the procedure developed in [46] are the two boundary functions $F_s(x, Q_0^2)$ and $G(x, Q_0^2)$, in the range $(x, 1)$ at the initial value $Q^2 = Q_0^2$. In the work in [16] we constructed $F_s(x, Q_0^2)$ from our analytic fit to the HERA data on $F_2^{\gamma p}$, using as extra input the singlet distribution T_8 from MSTW2008LO [55] and matching smoothly to results from either CTEQ6L [56] or MSTW2008LO for $x > 0.03$. Our results at small x are essentially independent of this region, and are determined by the known behavior of our Froissart-bounded fit at small x .

We chose $Q_0^2 = 4.5 \text{ GeV}^2$, a value in the region where the data are dense, and determined the gluon distribution $G(x, Q_0^2)$ in terms of $F_2^{\gamma p}$ and its derivatives with respect to $\ln Q^2$ and x by inverting the evolution equation for $F_2^{\gamma p}$. The details are given in [16]. We then determined F_s and the non-singlet distributions T_{15} and T_{24} by numerically inverting the Laplace transforms in our analytic solution of the evolution equations in Laplace space using the techniques in [51–53], and solved for the resulting quark distributions. We show the results for the MSTW-matched u , c , and b distributions in Fig. 7.

The results for the quark distributions shown in Fig. 7 are strikingly large compared to those obtained in Sec. IV A, Fig. 3. The figure, plotted on a logarithmic scale, suggests somewhat misleadingly that the naive wee parton limit, in which all the quark distributions approach a common limit at small x and large Q^2 with $xq_i(x, Q^2) \rightarrow xq(x, Q^2)$, $i = u, \bar{u}, \dots, b, \bar{b}$, holds in a perturbative treatment. Thus, while xc and xb differ from xu by about 4.5% and 11.5% at $v = 18.4$ ($x = 10^{-8}$), the two are within a half percent and 2% of xu at $v = 32.2$ ($x = 10^{-14}$), with the fractional difference still decreasing. The light quark PDFs $xd, x\bar{d}, xu, x\bar{u}$, are indistinguishable at the level of a tiny fraction of a percent level for small x , while $xs = x\bar{s}$ are within a percent to fraction of a percent of xu .

However, the actual distributions do *not* converge to a common limit as assumed in the naive wee parton picture, but again diverge from each other as $v^2 = \ln^2(1/x)$ with increasing v as required by the behavior of the initial (and evolved) non-singlet distributions T_{15} and T_{24} . The *fractional* differences converge in LO only because F_s grows asymptotically as $\exp[\text{constant} \times \sqrt{\tau v}]$ in LO for large Q^2 and large v . The ratio T_j/F_s therefore decreases sharply, and the differences between different quark distributions decrease strongly as *fractions* of the average distribution. This behavior is sufficient to ensure that the relation $F_2^{\nu(\bar{\nu})} \approx (45/11)F_2^{\gamma p}$ between the electromagnetic and neutrino structure functions continues to be satisfied to high fractional accuracy in LO even though the wee limit is not satisfied.

In Fig. 8, we compare the x -dependence of $F_2^{\gamma p}(x, M_Z^2)$ that results from evolving the quarks in LO from $Q_0^2 = 4.5 \text{ GeV}^2$ to M_Z^2 , with that found by evaluating the global fit to HERA data [17], Eq. (2), at $Q^2 = M_Z^2$ over the same range of x . In the region of the HERA data, $v \lesssim 10$, $Q^2 \lesssim 1000 \text{ GeV}^2$, the two versions of $F_2^{\gamma p}$ agree reasonably well, typically to $\sim 5\%$ as seen in Figs. 6 and 7 of [16]. However, there are systematic deviations of the LO result from the data which increase at large Q^2 ; a result of this trend is evident in Fig. 8, where the LO result falls noticeably below the fit at $Q^2 = M_Z^2$, a value well above those reached in the HERA data. We note also that the χ^2 of our fit to the data with $Q^2 \geq 2.7 \text{ GeV}^2$ is substantially better than that of the best LO result, 295 for 296 degrees of freedom as

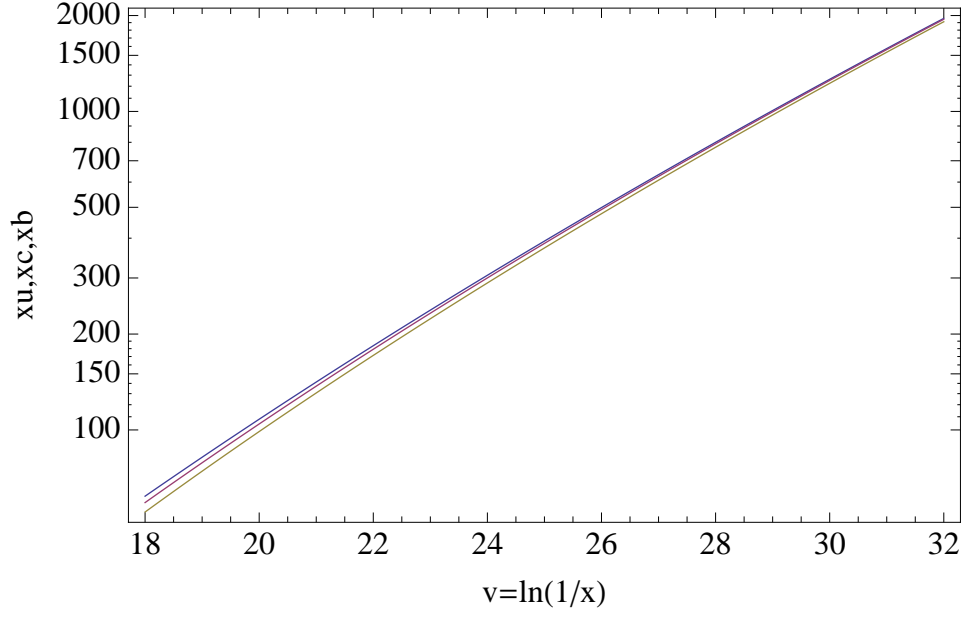


FIG. 7: The ultra low x behavior of the LO quark distributions xu , xc and xb at $Q^2 = M_Z^2/3$ for boundary functions derived from the Froissart-bounded fit to $F_2^{\gamma p}$ at $Q_0^2 = 4.5 \text{ GeV}^2$ as described in [16]. Top to bottom at $v = 18.4$ ($x = 10^{-8}$), xu , xc and xb .

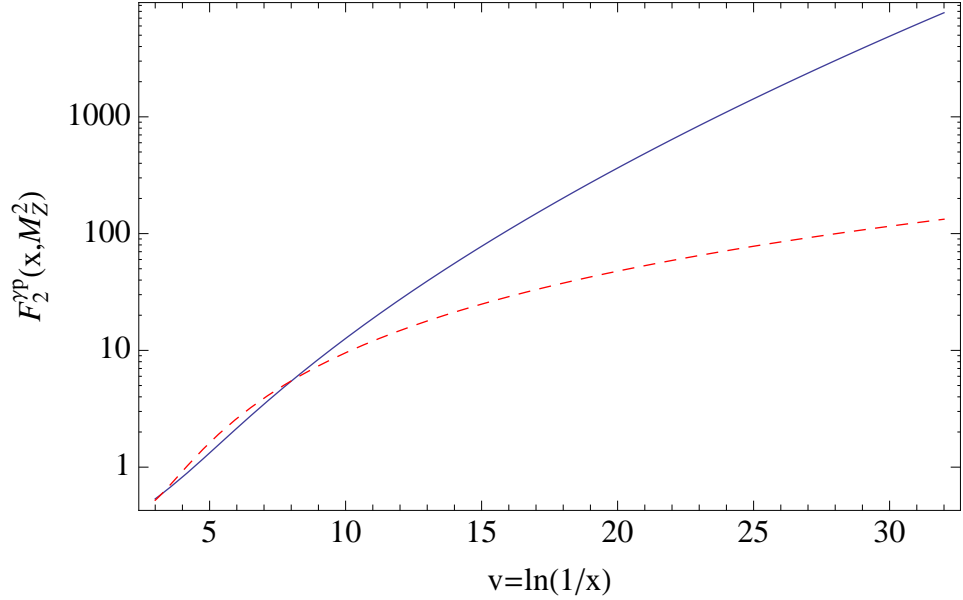


FIG. 8: The comparison of the results for $\hat{F}_2^{\gamma p}(x, M_Z^2)$ obtained using the LO BDHM quarks of [16] (solid blue curve), and those calculated directly from the Froissart-bounded fit function, Eq. (2) (dashed red curve), as a function of $v = \ln(1/x)$. The interval shown, $3 \leq v \leq 32.2$ corresponds to $0.05 \geq x \geq 10^{-14}$.

compared to 502 (1480) for the LO fit matched to MSTW2008 (CTEQ6L) at large x , or $\chi^2/\text{d.o.f.} \approx 1$ compared to 1.7 (5).

The evolved LO distribution for $F_2^{\gamma p}$ is clearly *not* consistent with the expected Froissart-bounded behavior at large v . While NLO corrections are known to be large and may damp the growth of the gluon distribution and $F_2^{\gamma p}$ at small x , the large deviation of the LO results from those given by our Froissart-bounded fit to the data suggests that a perturbative description may well fail, and that nonperturbative effects are likely to become important at ultra-small x .

D. Uncertainties in extrapolations of quark distributions

A different source of uncertainty in standard analyses which affects predictions for neutrino cross sections at very high energies is the use of arbitrary, often power-law based, parametrizations of input PDFs that cannot be extended reliably to small x , a problem we have avoided by working directly with $F_2^{\gamma p}$, which we assume can be extrapolated reasonably to small x using a theoretically consistent, Froissart-bounded form. To illustrate the problems that can be caused by the extension of typical parametrizations outside the region of the HERA data, we compare the present results with those of a LO pQCD analysis based on the parametrizations used in the comprehensive MSTW paper [55]. We use their MSTW2008LO parton parameterizations with the published parameter values to determine their boundary functions at $Q_0^2 = 1 \text{ GeV}^2$. MSTW numerically solved the coupled DGLAP equations on a fixed grid, $10^{-6} < x \leq 1$, $1 < Q^2 \leq 10,000 \text{ GeV}^2$, and fixed the parameters by matching the results to data.

We are primarily interested in the behavior of PDFs parametrized this way well below their grid limit on x , $x \geq 10^{-6}$. We assume that the same *ad hoc* starting expressions, satisfactory on their grid, can be extended to $x = 10^{-14}$ region, an obvious source of potential problems. For example, the MSTW2008LO fit function for the gluon PDF uses a single inverse power of x , $xg(x, Q_0^2) \propto x^{-0.837}$, to handle the small x description, a Froissart-violating form that dominates the evolution at small x and drives the behavior of the quark distributions [57]. Such assumed power-law dominated forms for the gluon distribution are common in the literature.

We solve directly for the quark PDFs using the same methods as above, but in terms of the MSTW2008LO input functions instead of those derived from our fit to $F_2^{\gamma p}$. In Fig. 9, we display the resulting small x behavior of the up, charm and bottom quark distributions at $Q^2 = M_Z^2$ over the range from $x = 10^{-14}$ up to $x = 10^{-8}$. The $u, \bar{u}, d, \bar{d}, s$ and \bar{s} quarks are indistinguishable on the scale of the figure. For fixed Q^2 , the quark PDFs rise as an inverse power law $xq \propto x^{-0.81}$ as x decreases, are many orders of magnitude larger at small x than those obtained in our earlier analysis, Fig. 3, and in our LO analysis starting with boundary functions determined by $F_2^{\gamma p}$ at $Q_0^2 = 4.5 \text{ GeV}^2$, Fig. 7. They are presumably unrealistically large.

A second remarkable feature of Fig. 9 is that the c and b quarks *never converge* to the others, all rising with the same approximate power law, but with different normalizations at large v . The quark distributions are *not* consistent with the wee parton picture, since the ratios of different quark distributions are fixed, and the different distributions do not converge toward a common value but actually *diverge* from each other as a power of $1/x$ as $x \rightarrow 0$.

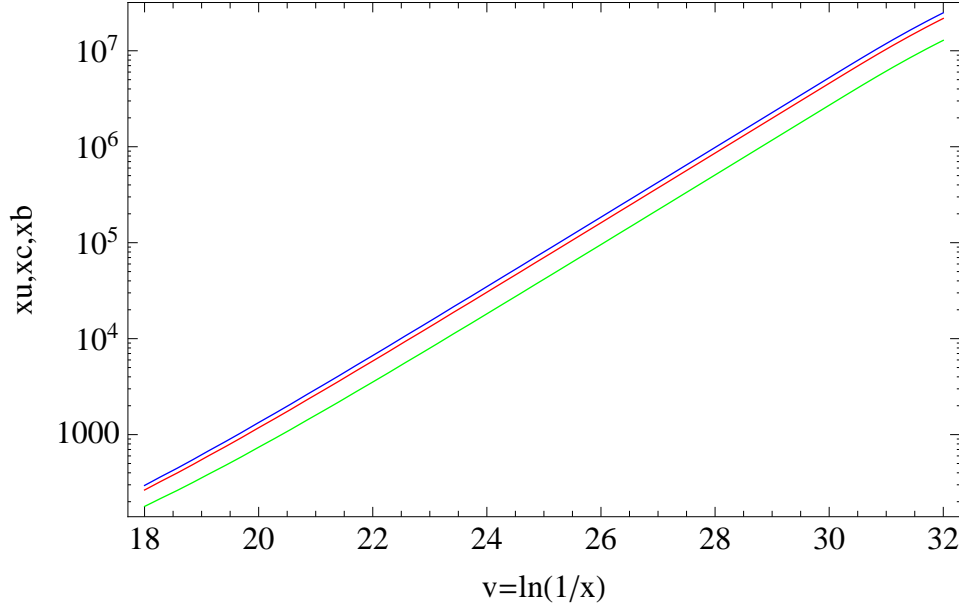


FIG. 9: Leading-order solutions for ux , xc , and xb at $Q^2 = M_Z^2/3$ as functions of $v = \ln(1/x)$ for initial gluon and quark distributions defined by extending the MSTW2008LO parametrizations, as given, from the HERA region to the ultra-small x region below $x = 10^{-8}$, $v > 18.4$. Top to bottom, ux , xc , and xb .

The power-law growth of the quark distributions at small x is what is expected for an $x^{-0.84}$ power-law input for the gluon since the gluon drives the small x behavior of the quark distributions [57]. The divergence in G at small x is sufficiently strong that it already dominates the very small x behavior of F_s at $Q^2 = m_c^2$, the threshold for charm production where F_s determines the initial non-singlet distribution T_{15} , $T_{15}(x, m_c^2) = F_s(x, m_c^2)$. As a result,

the gluon power divergence at small x is passed on to the difference between the charm and light quark PDFs even though there is no direct coupling of T_{15} to the gluon. The same is true, with increased effect, at the b threshold, so $xb(x, Q^2)$ also rises with approximately the same power for $x \rightarrow 0$ as is evident in Fig. 9, and the ratios of the quark PDFs do not converge as required in the wee limit.

As a result of this universal behavior, $F_2^{\gamma p}$ and the neutrino-nucleon structure function $F_2^{\nu(\bar{\nu})}$ show the same gluon-driven power law growth at small x . In terms of our discussion in Sec. II, the virtual gauge boson-nucleon cross sections rise with \hat{s} as \hat{s}^a with $a \sim 0.8$, in radical violation of the Froissart bound [19–22], a behavior which illustrates the danger in extending *ad hoc* parametrizations outside the region in which they are constrained by data.

A related problem appears in the extrapolation of quark PDFs from the experimental region to very small x when this is done by matching assumed forms without a firm theoretical basis to the fitted PDFs near the boundary of the experimental region. For example, the form $a + b \ln(1/x)$ used to extrapolate the published NLO MSTW quark distributions from the limiting grid value of 10^{-6} in MSTW2008 to the values $\sim 10^{-10}$ needed in the calculation of neutrino cross sections in [58], is inconsistent with the power law rise of the actual LO and NLO “MSTW” quark PDFs at ultra-small x . In the LO case checked here, the function used leads to a major underestimate of the extrapolated LO distributions and the corresponding high energy cross sections relative to those obtained in the direct (but unrealistic) LO calculation. Interestingly, the extrapolation of the NLO PDFs in [58] still gives a cross section larger than that obtained using our Froissart-bounded extrapolation of $F_2^{\gamma p}$, quadratic rather than linear in $\ln(1/x)$, and the relation $F_2^{\nu(\bar{\nu})} \approx (45/11)F_2^{\gamma p}$; this is presumably the result of matching to the rapid growth of the power-law variation of the MSTW quarks, and the limited range of the extrapolation.

V. CONCLUSIONS

We have investigated the results that follow from the assumption that the cross section for the scattering of a virtual photon with $q^2 = -Q^2 < 0$ from a nucleon, hence the structure function $F_2^{\gamma p}$ in deep inelastic $e^\pm p$ scattering, is hadronic in nature with the same Froissart-bounded structure as is observed in hadronic and real γp scattering. We have presented theoretical arguments in favor of this assumption, which is supported experimentally by the very accurate fit to the HERA data on $F_2^{\gamma p}$ obtained in earlier work. This fit is quadratic in the natural variable $v = \ln(1/x)$ for x small, and allows a reliable extrapolation of $F_2^{\gamma p}$ to ultra low values of x .

We have used this fit in conjunction with information on the small non-singlet function T_8 and the gluon distribution extrapolated consistently from results of the CT10 analysis of the HERA data [47] to derive a complete set of quark distributions for $n_f = 5$ active quarks for $x > 10^{-14}$ or $v < 32$. The derivation does *not* use the DGLAP equations, which are expected to break down at very small x [31]. These quark distributions do not show the limiting behavior expected in the wee parton picture, in which the deviations of the distributions from one another tend to zero at small x and large Q^2 , but actually diverge for $x \rightarrow 0$.

We show that, despite the failure of the wee parton picture at the quark level, the relations between $F_2^{\gamma p}$ and the dominant structure functions $F_2^{\nu(\bar{\nu})}$ and $F_0^{\nu(\bar{\nu})}$ in charged- and neutral-current neutrino scattering derived in the wee parton picture continue to hold to high accuracy at very small x . With this established, the use of the (supposed) wee parton relations to predict the dominant neutrino structure function $F_2^{\nu(\bar{\nu})}$ in terms of $F_2^{\gamma p}$ gives results that are *independent* of assumptions about the gluon distribution, and appear to hold quite generally. These relations are exploited in the accompanying paper [13]. The neutrino cross sections will be accessible at energies E_ν up to 10^{17} GeV in planned neutrino observatories, requiring values of x down to $x = 10^{-14}$. This corresponds to a relatively modest extrapolation by a factor of ~ 3 in v from the upper values $v \sim 10$ explored at HERA to the values $v \sim 30$ needed for $E_\nu \sim 10^{17}$ GeV. We emphasize that, through the connections established here, measurements of the neutrino cross sections would allow, through the structure functions, the exploration of *hadronic* interactions at energies not otherwise accessible.

As part of our analysis, we obtain simple analytic expressions for the effects of non-singlet DGLAP evolution on the functions T_8 , T_{15} , and T_{24} needed in the derivation of quark distributions, and of the effects of the NLO QCD corrections needed to transform between the LO-type expressions for $F_{20}^{\gamma p}$ in terms of quark distributions, and the physical $F_2^{\gamma p}$.

We also compared our general results to those obtained in a LO analysis based on boundary functions obtained up to the small non-singlet term T_8 entirely from our Froissart-bounded fit to the HERA data. The LO results are markedly larger at very small x and large Q^2 , and are not consistent with the extrapolated fit. There is again no proper wee parton limit for the quark distributions.

Finally, to illustrate the difficulties that can ensue from the extrapolation of the *ad hoc* parametrizations of parton distributions used in standard analyses of deep inelastic scattering out of the experimental domain where the parameters are determined, we calculated the “MSTW” quark distributions which follow from a direct extension to very

small x of the analytic expressions used to specify the initial boundary distributions in the MSTW2008LO fit to $F_2^{\gamma p}$. The results are drastically different from the Froissart-bounded results found here, and also from the $a + b \ln(1/x)$ extrapolations of the fitted distributions MSTW distributions used in the prediction of neutrino cross sections in [58]. It appears to be far better to extrapolate $F_2^{\gamma p}$ directly, and use the results to determine boundary functions for a DGLAP analysis, or, as here, to determine the PDFs from the extrapolated global fit to the v - and Q^2 -dependent data.

We conclude that the cross sections and quark distributions calculated from the small x , large Q^2 extrapolation of $F_2^{\gamma p}(x, Q^2)$ from our saturated Froissart-bounded fit to the HERA data are the most physically motivated, are consistent with all other hadronic cross sections including γp , and provide the best estimate of the UHE energy neutrino-nucleon cross sections, which we develop fully in Part II [13].

Acknowledgments

M. M. B. and L. D. would like to thank the Aspen Center for Physics, where this work was supported in part by NSF Grant No. 1066293, for its hospitality. M. M. B. would like to thank Prof. A. Vainshtein for valuable discussions. P. H. would like to thank Towson University Fisher College of Science and Mathematics for support. D. W. M. receives support from DOE Grant No. DE-FG02-04ER41308.

Appendix: Calculation of $F_{2,0}^{\gamma p}$

We recall that the structure function $F_2^{\gamma p}$ is given in terms of the quark-level expression $F_{20}^{\gamma p}$ in Eq. (17) by convolution with a set of coefficient functions from the operator product expansion [41, 42],

$$x^{-1} F_2^{\gamma p} = \left[\mathbb{1} + \frac{\alpha_s}{2\pi} C_{2q} \right] \otimes (x^{-1} F_{2,0}^{\gamma p}) + \frac{\alpha_s}{2\pi} \left(\sum_i e_i^2 \right) C_{2g} \otimes g, \quad (\text{A.1})$$

where the convolution \otimes of operators A and B is defined as

$$A \otimes B = \int_x^1 \frac{dz}{z} A(x/z) B(z) = \int_x^1 \frac{dz}{z} A(z) B(x/z). \quad (\text{A.2})$$

The operator $\mathbb{1}$ in Eq. (A.1) is the unit operator and the sum over charges in the second term runs over active quarks and antiquarks.

The coefficient functions C_{2q} and C_{2g} depend on the renormalization scheme used in perturbative calculations and the order to which they are carried. We assume the use of the standard $\overline{\text{MS}}$ scheme in which, at NLO [39],

$$C_{2q} = \frac{4}{3} \left[- \left(\frac{\pi^2}{3} + \frac{9}{2} \right) \delta(1-z) + 2 \left(\frac{\ln(1-z)}{1-z} \right)_+ - \frac{3}{2} \left(\frac{1}{1-z} \right)_+ + 3 + 2z - (1+z) \ln(1-z) - \frac{1+z^2}{1-z} \ln z \right], \quad (\text{A.3})$$

$$C_{2g} = \frac{1}{2} \left[\left((1-z)^2 + z^2 \right) \ln \frac{1-z}{z} - 8z^2 + 8z - 1 \right]. \quad (\text{A.4})$$

The coupling $\alpha_s(Q^2)$ is to be evaluated at the same order.

The expression in Eq. (A.1) is usually used to determine $x^{-1} F_2^{\gamma p}$ from the individual quark and gluon distributions found in fits to the DIS data. However, the relation can also be inverted to determine $x^{-1} F_{2,0}^{\gamma p}$ directly at a given order in α_s in terms of the observable structure function $x^{-1} F_2^{\gamma p}$ and a given gluon distribution $g(x, Q^2)$, i.e.,

$$x^{-1} F_{20}^{\gamma p} = \left[\mathbb{1} + \frac{\alpha_s}{2\pi} C_{2q} \right]^{-1} \otimes \left(x^{-1} F_2^{\gamma p} - \frac{\alpha_s}{2\pi} \left(\sum_i e_i^2 \right) C_{2g} \otimes g \right). \quad (\text{A.5})$$

This is the result we need to obtain the singlet quark distribution F_s and individual quark distributions as outlined in Sec. III A. As discussed there, F_s is determined (except at very low Q^2) by $F_{20}^{\gamma p}$ and the non-singlet functions T_{15} and T_{24} , themselves related to F_s .

We sketch here the evaluation of the inverse operator and the final expression in Eq. (A.5) using Laplace transform. This requires several steps. We first multiply by x and use the second form of Eq. (A.2) to recast Eq. (A.1) in the form

$$F_2^{\gamma p}(x, Q^2) = \left[\mathbb{1} + \frac{\alpha_s}{2\pi} (z C_{2q}) \right] \otimes F_{20}^{\gamma p} + \frac{\alpha_s}{2\pi} + \left(\sum_i e_i^2 \right) (z C_{2g}) \otimes G \quad (\text{A.6})$$

$$= F_{20}^{\gamma p}(x, Q^2) + \frac{\alpha_s}{2\pi} \int_x^1 \frac{dz}{z} \left[z C_{2q}(z) F_{20}^{\gamma p}(x/z, Q^2) + \left(\sum_i e_i^2 \right) z C_{2g}(z) G(x/z, Q^2) \right], \quad (\text{A.7})$$

where $G(x, Q^2) = xg(x, Q^2)$. We next transform the terms in Eq. (A.3) that involve distributions. Since $F(x/z) \equiv F_2^{\gamma p}(x/z, Q^2) \equiv 0$ for $z < x$, we may take the lower limit of integration in the convolution as 0, and write

$$\int_x^1 dz F(x/z) \frac{1}{(1-z)_+} = \int_0^1 dz \frac{F(x/z)}{(1-z)_+} \quad (\text{A.8})$$

$$\equiv \int_0^1 dz \frac{F(x/z) - F(x)}{1-z} \quad (\text{A.9})$$

$$= F(x) \ln(1-x) + \int_x^1 dz \frac{F(x/z) - F(x)}{1-z} \quad (\text{A.10})$$

$$= F(x) \ln \frac{1-x}{x} + x \int_x^1 \left(\frac{F(y)}{y} - \frac{F(x)}{x} \right) \frac{dy}{y-x} \quad (\text{A.11})$$

$$= \int_0^v dw \ln(1 - e^{-(v-w)}) \frac{\partial \hat{F}(w)}{\partial w}, \quad (\text{A.12})$$

where we have used the definition of the “+” operation in Eq. (A.9), evaluated the integral on the interval $(0, x)$, changed the integration variable z to $y = x/z$ in Eq. (A.11), and finally introduced the natural variables $v = \ln(1/x)$ and $w = \ln(1/y)$ and integrated by parts in Eq. (A.12) using a limiting procedure as sketched in [46]. The function $\hat{F}(w)$ is defined as $\hat{F}(w) \equiv \hat{F}_{20}^{\gamma p}(w, Q^2) = F_{20}^{\gamma p}(e^{-w}, Q^2)$.

A similar calculation for the term in Eq. (A.3) proportional to $(\ln(1-z)/(1-z))_+$ gives

$$\int_x^1 dz F(x/z) \left(\frac{\ln(1-z)}{(1-z)} \right)_+ = \int_0^v dw \ln^2(1 - e^{-(v-w)}) \frac{\partial \hat{F}(w)}{\partial w}. \quad (\text{A.13})$$

Using these results and transforming the remaining terms in Eq. (A.7) to v space, we obtain the expression

$$\begin{aligned} \hat{F}_2^{\gamma p}(v, Q^2) &= \hat{F}_{20}^{\gamma p}(v, Q^2) + \frac{\alpha_s(Q^2)}{2\pi} \left\{ - \left(6 + \frac{4}{9}\pi^2 \right) \hat{F}_{20}^{\gamma p}(v, Q^2) + \int_0^v dw \hat{H}_q(v-w) \hat{F}_{20}^{\gamma p}(w, Q^2) \right. \\ &\quad \left. + \int_0^v dw \left[\frac{8}{3} \ln^2(1 - e^{-(v-w)}) - 4 \ln(1 - e^{-(v-w)}) \right] \frac{\partial \hat{F}_{20}^{\gamma p}(w, Q^2)}{\partial w} \right\} \\ &\quad + \frac{\alpha_s(Q^2)}{2\pi} \left(\sum_i e_i^2 \right) \int_0^v dw \hat{H}_g(v-w) \hat{G}(w, Q^2). \end{aligned} \quad (\text{A.14})$$

Here $\hat{G}(w, Q^2) = G(e^{-w}, Q^2)$. The functions \hat{H}_q and \hat{H}_g are defined as

$$\hat{H}_q(v) = e^{-v} C'_{2q}(e^{-v}), \quad (\text{A.15})$$

$$\hat{H}_g(v) = e^{-v} C_{2g}(e^{-v}), \quad (\text{A.16})$$

where $C'_{2q}(z)$ contains the terms in C_{2q} other than the delta function and the “+” terms treated above, i.e.,

$$C'_{2q}(z) = \frac{4}{3} \left[3 + 2z - \frac{1+z^2}{1-z} \ln z - (1+z) \ln(1-z) \right]. \quad (\text{A.17})$$

The right-hand side of Eq. (A.14) is a sum of convolutions in v space, and can be factored by Laplace transformation into a sum of the products of the transforms of the functions in those convolutions,

$$f_2(s) = f_{20}(s) + \frac{\alpha_s}{2\pi} f_{20}(s) \left(-6 - \frac{4}{9}\pi^2 + h_{q1}(s) + s h_{q2}(s) \right) + \frac{\alpha_s}{2\pi} \left(\sum_i e_i^2 \right) \tilde{g}(s) h_g(s). \quad (\text{A.18})$$

Here $f_{20}(s)$, $f_2(s)$, and $\tilde{g}(s)$ are the Laplace transforms of \hat{F}_{20} , \hat{F}_2 , and \hat{G} with respect to v , with their Q^2 dependence suppressed,

$$f_{20}(s) = \mathcal{L} \left[\hat{F}_{20}^{\gamma p}(v, Q^2); s \right], \quad (\text{A.19})$$

$$f_2(s) = \mathcal{L} \left[\hat{F}_2^{\gamma p}(v, Q^2); s \right], \quad (\text{A.20})$$

$$\tilde{g}(s) = \mathcal{L} \left[\hat{G}(v, Q^2); s \right], \quad (\text{A.21})$$

while

$$\begin{aligned} h_{q1}(s) &= \mathcal{L} \left[\hat{H}_q(v); s \right] \\ &= \frac{4}{3} \left(\frac{H_{s+1} + 3}{s + 1} + \frac{H_{s+2} + 2}{s + 2} + \zeta(2, s + 1) + \zeta(2, s + 3) \right), \end{aligned} \quad (\text{A.22})$$

$$\begin{aligned} s h_{q2}(s) &= s \mathcal{L} \left[\frac{8}{3} \ln^2(1 - e^{-v}) - 4 \ln(1 - e^{-v}); s \right] \\ &= \frac{8}{3} \left(\frac{\pi^2}{6} + (H_s)^2 - \psi'(s + 1) \right) + 4H_s, \end{aligned} \quad (\text{A.23})$$

$$\begin{aligned} h_g(s) &= \mathcal{L} \left[\hat{H}_g(v); s \right] \\ &= -\frac{1}{2} \frac{H_s + 1}{s + 1} + \frac{H_{s+1} + 4}{s + 2} - \frac{H_{s+2} + 4}{s + 3}. \end{aligned} \quad (\text{A.24})$$

In these expressions, $H_s = \psi(s + 1) - \psi(1)$, $\psi(s) = \Gamma'(s)/\Gamma(s)$, and $\zeta(2, s) = \sum_{k=0}^{\infty} (k + s)^{-2}$ is the Hurwitz generalized zeta function of degree 2. The factor s which multiplies $h_{q2}(s)$ in Eq. (A.18) and Eq. (A.23) arises from the derivative of $\hat{F}_{20}^{\gamma p}$ in Eq. (A.14) and the relation $\mathcal{L}[\partial f(w)/\partial w; s] = s \mathcal{L}[f(w); s]$.

In the expression in Eq. (A.18), $f_2(s)$ is known from our fit to the HERA data, and $g(s)$ is assumed also to be known, for example, from the extension of $G(x, Q^2)$ from earlier parton level fits to the data as extended to small x . Solving for $f_{20}(s)$, we find that

$$f_{20}(s) = \left[f_2(s) - \frac{\alpha_s}{2\pi} \left(\sum_i e_i^2 \right) h_g(s) \tilde{g}(s) \right] / [1 + (\alpha_s/2\pi)d(s)], \quad (\text{A.25})$$

where

$$d(s) = -6 - \frac{4}{9}\pi^2 + h_{q1}(s) + s h_{q2}(s). \quad (\text{A.26})$$

Thus, inverting the Laplace transform in Eq. (A.19), we find that

$$\begin{aligned} \hat{F}_{20}^{\gamma p} &= \mathcal{L}^{-1} [f_{20}(s); v] \\ &= \mathcal{L}^{-1} \left[\frac{f_2(s)}{1 + (\alpha_s/2\pi)d(s)} - \frac{\alpha_s}{2\pi} \left(\sum_i e_i^2 \right) \frac{h_g(s) \tilde{g}(s)}{1 + (\alpha_s/2\pi)d(s)}; v \right]. \end{aligned} \quad (\text{A.27})$$

The inverse Laplace transform in Eq. (A.27) can be calculated simply analytically for v large or x small. In particular, in our Froissart bounded model, $\hat{F}_2^{\gamma p}(v, Q^2)$ and $\hat{G}(v, Q^2)$ are essentially quadratic polynomials in v for $v \gg 1$ as in Eq. (4). In the polynomial terms, $v^n \rightarrow n!/s^{n+1}$ under Laplace transformation. The exponentially small terms omitted in Eq. (4) give extra poles for $s \rightarrow -1, -2, \dots$, and, if retained, lead only to terms of order e^{-v} or smaller in the final result. The main contributions for $n_f = 5$ and $v \gg 1$ are therefore given by integrals of the form

$$\frac{n!}{2\pi i} \int_{-i\infty+\epsilon}^{i\infty+\epsilon} \frac{ds}{s^{n+1}} e^{vs} \frac{[1, (\alpha_s/2\pi)(22/9)h_g(s)]}{1 + (\alpha_s/2\pi)d(s)}, \quad n = 0, 1, 2, \quad (\text{A.28})$$

where the numerator function in Eq. (A.28) is 1 for the f_2 term in Eq. (A.27) and $(\alpha_s/2\pi)(22/9)h_g(s)$ for the g term.

The numerator functions have no singularities in the complex plane to the right of $s = -1$. The function $d(s)$ has second-order poles for $s \rightarrow -1, -2, -3, \dots$, but these cause no problems. However, the complete denominator

function has a pair of complex conjugate zeros near and to the right of -1 where

$$(s+1)^2 [1 + (\alpha_s/2\pi)d(s)] \rightarrow (s+1)^2 \left[1 - \frac{\alpha_s}{2\pi} \left(\frac{10}{3} + \frac{2\pi^2}{3} \right) \right] + \frac{4}{3} \frac{\alpha_s}{2\pi} + \frac{2}{9} \frac{\alpha_s}{2\pi} [4\pi^2 - 12 - 21\psi''(1) - 24\zeta(3)] (s+1)^3 + \dots, \quad (\text{A.29})$$

leading (in order α_s) to complex conjugate poles at

$$s \approx -1 + O(\alpha_s^2) \pm i \left[\frac{\alpha_s}{2\pi} \left(\frac{10}{3} + \frac{2\pi^2}{3} \right) \right]^{1/2} [(1 + O(\alpha_s))], \quad (\text{A.30})$$

e.g., at $s = -0.9962 \pm 0.1750 i$ for $\alpha_s(M_Z^2) = 0.118$. There are further pairs of conjugate poles near $s = -2, -3, \dots$. These pole positions will be shifted slightly and new poles introduced when the coefficient functions C_{2q} and C_{2g} are evaluated to higher orders in α_s , introducing higher order contributions in $1/(s+1)$, but the rightmost singularities from the (generalized) factor $1/[1 + (\alpha_s/2\pi)d(s)]$ should remain very close to $s = -1$.

We conclude that the contours of integration in Eq. (A.28) can be shifted to the left in the complex s plane as in Fig. 1 to run through saddle points close to $s = -1$, but just to the right of the complex conjugate poles in Eq. (A.30), picking up the residues of the integrands at $s = 0$ and leaving a residual integral which is suppressed by a factor $\approx e^{-v}$, very small for v large. We drop the latter.

The calculation of the residues of the poles at $s = 0$ is straightforward. Thus, for the “1” term in Eq. (A.28), the quadratic form of our input function $\hat{F}_2^{\gamma p}(v)$ in v is reproduced in $\hat{F}_{20}^{\gamma p}(v)$ with small shifts in v and an added constant in the v^2 term as given below in Eqs. (A.31) and (A.32). The analytic forms of the coefficients in these expressions are known, but are too complicated to record here. Similar results hold for the “ g ” term.

Combining the results, we find that, for general values of $b(Q^2) = \alpha_s(Q^2)/2\pi$,

$$\begin{aligned} \hat{F}_{20}^{\gamma p}(v, Q^2) &= \hat{F}_2^{\gamma p}(v_f, Q^2) - (5.523 - 17.665b) b \hat{C}_{2f}(Q^2) \\ &\quad - \frac{11}{27} b \hat{G}(v_g, Q^2) + \frac{11}{27} b (7.549 + 5.523b - 17.665b^2) \hat{C}_{2g}(Q^2) + O(e^{-v}), \end{aligned} \quad (\text{A.31})$$

to NLO, where $\hat{C}_{2f}(Q^2)$ is the coefficient of v^2 in $F_2^{\gamma p}(v, Q^2)$, Eqs. (4) and (7), and $\hat{C}_{2g}(Q^2)$ is the coefficient of the corresponding term in $\hat{G}(v, Q^2)$. The shifted arguments v_f and v_g are

$$v_f = v - 4.203b, \quad v_g = v - 4.623 - 4.203b. \quad (\text{A.32})$$

The main uncertainty in the overall result for $\hat{F}_{20}^{\gamma p}$ arises from the uncertainty in the gluon distribution. This was treated as in Sec. IV using an extrapolation of the CT10 [47] $G(x, Q^2)$ quadratic in v , with coefficients quadratic in $\ln Q^2$, fitted to the NNLO G over the region $2 \times 10^{-4} \leq x \leq 0.01$, $10 \text{ GeV}^2 \leq Q^2 \leq 1000 \text{ GeV}^2$. As noted earlier, this agrees very well with the HERAPDF version of G .

We emphasize that the form of these results, with quadratics in v transformed to quadratics up to exponentially small corrections, is quite general, the result simply of the calculation of residues at $s = 0$, with all other singularities of the integrands, from either the kernel functions in Laplace space or the forms of $\hat{F}_2^{\gamma p}$ or \hat{G} for $v \sim 0$, displaced at least to the vicinity of $s = -1$.

The calculation of the neutrino structure functions $F_2^{\nu(\bar{\nu})}$ and $F_0^{\nu(\bar{\nu})}$ also requires the evaluation of the action of $[1 + (\alpha_s/2\pi)C_{2q}]$ on the functions T_8 , T_{15} , and T_{24} . In v space, these are quadratics in v for v large. The resulting transformation of the powers v^n , $n = 0, 1, 2$ is just the inverse of that associated with the “1” term in the transformation $\hat{F}_2^{\gamma p} \rightarrow \hat{F}_{20}^{\gamma p}$ discussed above; \hat{G} does not enter. Thus,

$$\hat{T}_i(v, Q^2) \rightarrow \hat{T}_i(v_T, Q^2) + (5.523 - 17.665b) b \hat{C}_{2,T_i}(Q^2), \quad v_T = v + 4.203b, \quad (\text{A.33})$$

with $\hat{C}_{2,T_i}(Q^2)$ the coefficient of the quadratic term in v in $T_i(v, Q^2)$. The functions $\hat{T}_i(v, Q^2)$ are given in terms of the initial distributions $T_i(v, Q_0^2)$ determined at $Q_0^2 = m_c^2, m_b^2$ by the expression in Eqs. (28), (40), and (41).

The calculation of the complete neutrino cross sections also requires the structure functions xF_3 and F_L . These are given to NLO, using the form analogous to that for $F_2^{\gamma p}$ in Eq. (A.6), by

$$xF_3^{\nu(\bar{\nu})} = xF_{3,0}^{\nu(\bar{\nu})} + \frac{\alpha_s}{2\pi} (zC_{3q}) \otimes (zF_{3,0}^{\nu(\bar{\nu})}), \quad (\text{A.34})$$

$$F_L^{\nu(\bar{\nu})}(x, Q^2) = \frac{\alpha_s}{2\pi} (zC_{Lq}) \otimes F_{20}^{\nu(\bar{\nu})} + \frac{\alpha_s}{2\pi} 2n_f (zC_{Lg}) \otimes G. \quad (\text{A.35})$$

where, for example, $F_{3,0}^\nu = u + d + 2s + 2b - \bar{u} - \bar{d} - 2\bar{c}$ for $n_f = 5$. The coefficient functions are

$$C_{3q}(z) = C_{2q}(z) - \frac{4}{3}(1+z), \quad C_{3g} = 0 \quad (\text{A.36})$$

$$C_{Lq}(z) = \frac{8}{3}z, \quad C_{Lg}(z) = 2z(1-z). \quad (\text{A.37})$$

Transforming Eq. (A.34) to v space and factoring the resulting convolution with a Laplace transform, we find that

$$f_3 = [\mathbb{1} + bd(s) + bh_{3q}(s)] f_{30}. \quad (\text{A.38})$$

where f_3 and f_{30} are the Laplace transforms of \hat{F}_3 and \hat{F}_{30} with respect to v , and

$$h_{3q}(s) = -\frac{4}{3} \left(\frac{1}{s+1} + \frac{1}{s+2} \right). \quad (\text{A.39})$$

Since \hat{F}_{30} is a quadratic in v for v large, we can calculate the inverse Laplace transform of f_3 as above by calculating the residues of the integrand $e^{vs} [\mathbb{1} + bd(s) + bh_{3q}(s)] (n!/s^{n+1})$ for $n = 0, 1, 2$, corresponding to inputs v^n . The results give

$$\hat{F}_3(v, Q^2) = (1-2b)\hat{F}_{30}(v_3, Q^2) + \frac{(2.523 - 39.499b)b}{1-2b} \hat{C}_{2,3}(Q^2) + O(e^{-v}), \quad (\text{A.40})$$

$$v_3 = v + \frac{5.870b}{1-2b}, \quad (\text{A.41})$$

to NLO, with $\hat{C}_{2,3}(Q^2)$ the coefficient of v^2 in $\hat{F}_{30}(v, Q^2)$.

Similarly, for F_L , we find that

$$f_L = bh_{Lq}(s)f_{20} + 2n_f b h_{Lg}(s)\tilde{g}, \quad (\text{A.42})$$

$$h_{Lq} = \frac{8}{3} \frac{1}{s+2}, \quad h_{Lg} = \frac{2}{s+2} - \frac{2}{s+3}, \quad (\text{A.43})$$

where \tilde{g} is the Laplace transform of $\hat{G}(v, Q^2)$. Using the quadratic forms of f_{20} and \tilde{g} in v and evaluating the residues at $s = 0$ in the inverse Laplace transform, we get

$$\begin{aligned} \hat{F}_L(v, Q^2) &= \frac{4b}{3} \hat{F}_{20} \left(v - \frac{1}{2}, Q^2 \right) + \frac{b}{3} \hat{C}_{2,f0} \\ &\quad + \frac{2n_f b}{3} \hat{G} \left(v - \frac{5}{6}, Q^2 \right) + \frac{13n_f b}{54} \hat{C}_{2g} + O(e^{-v}), \end{aligned} \quad (\text{A.44})$$

in NLO, with $\hat{C}_{2,f0}(Q^2)$ and $\hat{C}_{2g}(Q^2)$ the coefficients of v^2 in $\hat{F}_{20}(v, Q^2)$ and $\hat{G}(v, Q^2)$.

-
- [1] M. M. Block, E. L. Berger, and C.-I. Tan, Phys. Rev. Lett. **97**, 252003 (2006), hep-ph/0610296.
 - [2] E. L. Berger, M. M. Block, and C.-I. Tan, Phys. Rev. Lett. **98**, 242001 (2007), hep-ph/0703003.
 - [3] M. M. Block, E. L. Berger, D. W. McKay, and C.-I. Tan, Phys. Rev. D **77**, 053007 (2008P), arXiv: 0708.1960v1 [hep-ph].
 - [4] M. Block, P. Ha, and D. McKay, Phys. Rev. D **82**, 077302 (2010).
 - [5] M. M. Block, Phys. Rep. **36**, 71 (2006).
 - [6] ATLAS Collaboration, Nature Comm. **2**, 463 (2011).
 - [7] G. Antchev et al. (TOTEM Collaboration), Euro. Phys. Lett. **96**, 21002 (2011).
 - [8] CMS Collaboration, CERN Document Server, <http://cdsweb.cern.ch/record/1373466?ln=en>, 2011.
 - [9] P. Abreu et al. (Pierre Auger Collaboration), Phys. Rev. Lett. 062002 (2012) **109**, 062002 (2012), arXiv:1208.1520 [hep-ex].
 - [10] M. Block, Phys. Rev. D **84**, 091501 (2011).
 - [11] M. M. Block and F. Halzen, Phys. Rev. Lett. **107**, 212002 (2011).
 - [12] M. M. Block and F. Halzen, Phys. Rev. D **86**, 051504 (2012).
 - [13] M. M. Block, L. Durand, P. Ha, and D. W. McKay (2012), the companion paper, this journal.
 - [14] N. Letinien, P. Gorham, A. Jacobson, and R. Roussel-Dupré, Phys. Rev. D **69**, 013008 (2004).
 - [15] P. Gorham et al. (GLUE Collaboration), Phys. Rev. Lett. **93**, 041101 (2004).

- [16] M. M. Block, L. Durand, P. Ha, and D. W. McKay, Phys. Rev. D **84**, 094010 (2011).
- [17] F. D. Aaron et al. (H1 and ZEUS), JHEP **1001**, 109 (2010), arXiv:0911.0884 [hep-ex].
- [18] Ashok suri, Phys. Rev. D **4**, 570 (1971).
- [19] A. Martin, Phys. Rev. **129**, 1432 (1963).
- [20] Y. S. Jin and A. Martin, Phys. Rev. **135**, 1375 (1964).
- [21] A. Martin, Nuovo Cimento **42**, 930 (1966).
- [22] M. Froissart, Phys. Rev. **123**, 1053 (1961).
- [23] J. Sakurai, Ann. of Physics (NY) **11**, 1 (1960).
- [24] J. Sakurai, *Currents and Mesons* (Univ. of Chicago Press, 1969).
- [25] D. Schildknecht, Acta. Phys. Polon. **B37**, 595 (2006).
- [26] S. Adler and R. Dashen, *Current Algebras* (Benjamin, N.Y., 1968).
- [27] L. Durand, in *Design and Utilization of the Superconducting Supercollider, Snowmass 1984*, edited by P. Donaldson and J. Morfin (Division of Particles and Fields of the American Physical Society, 1985), p. 258.
- [28] P. L'Heureux, B. Margolis, and P. Valin, Phys. Rev. D **32**, 1681 (1985).
- [29] L. Durand and H. Pi, Phys. Rev. Lett. **58**, 303 (1987).
- [30] K. Honjo, L. Durand, R. Gandhi, H. Pi, and I. Sarcevic, Phys. Rev. D **48**, 1048 (1993).
- [31] L. Gribov, E. Levin, and M. Ryskin, Phys. Reports **100**, 1 (1983).
- [32] V. N. Gribov and L. N. Lipatov, Sov. J. Nucl. Phys. **15**, 438 (1972).
- [33] G. Altarelli and G. Parisi, Nucl. Phys. B **126**, 298 (1977).
- [34] Y. L. Dokshitzer, Sov. Phys. JETP **46**, 641 (1977).
- [35] J. Breitweg et al. (ZEUS Collaboration), Phys. Lett. B **487**, 53 (2000).
- [36] S. Chekanov et al. (ZEUS Collaboration), Eur. Phys. J. C **21**, 443 (2001).
- [37] C. Adloff et al. (H1 Collaboration), Eur. Phys. J. C **21**, 33 (2001).
- [38] M. M. Block, Nucl. Inst. and Meth. A. **556**, 308 (2006).
- [39] R. K. Ellis, W. J. Stirling, and B. R. Webber, *QCD and Collider Physics* (Cambridge University Press, 2003).
- [40] W. A. Bardeen, A. J. Buras, D. W. Duke, and T. Muta, Phys. Rev. D **18**, 3998 (1978).
- [41] R. Harrod and S. Wada, Phys. Lett. **96B**, 195 (1980).
- [42] W. Furmanski and R. Petronzio, Zeit. fur Physik **C11**, 293 (1982).
- [43] M. M. Block, L. Durand, and D. W. McKay, Phys. Rev. D **77**, 094003 (2008), arXiv:0710.3212 [hep-ph].
- [44] M. M. Block, L. Durand, and D. W. McKay, Phys. Rev. D **79**, 014031 (2009), arXiv:0808.0201 [hep-ph].
- [45] M. M. Block, L. Durand, P. Ha, and D. W. McKay, Eur. Phys. J. C **69**, 425 (2010), arXiv:1005.2556 [hep-ph].
- [46] M. M. Block, L. Durand, P. Ha, and D. W. McKay, Phys. Rev. D **83**, 054009 (2011), arXiv:1010.2486 [hep-ph].
- [47] H.-L. Lai, M. Guzzi, J. Huston, Z. Li, P. M. Nadolsky, J. Pumplin, and C.-P. Yuan, Phys. Rev. D **82**, 072024 (2010), arXiv:1007.2241[hep-ph].
- [48] <http://durpdg.dur.ac.uk/hepdata/pdf3.html>.
- [49] J. Beringer et al. (Particle Data Group), Phys. Rev. D **86**, 010001 (2012).
- [50] <http://pdg.lbl.gov/>.
- [51] M. M. Block, Eur. Phys. J. C **65**, 1 (2010).
- [52] M. M. Block, Eur. Phys. J. C **68**, 683 (2010), arXiv:1004:3585[hep-ph].
- [53] M. M. Block and L. Durand, Eur. Phys. J. C **71**, 1806 (2011).
- [54] M. M. Block, unpublished.
- [55] A. D. Martin, W. J. Stirling, R. S. Thorne, and G. Watt, Eur. Phys. J. C **63**, 189 (2009), arXiv:0901.0002 [hep-ph].
- [56] D. Stump, J. Huston, J. Pumplin, W. Tung, H. Lai, S. Kuhlmann, and J. Owens, J. High Energy Phys. **0310**, 046 (2003), [hep-ph/0303013].
- [57] D. W. McKay and J. Ralston, Nucl. Phys. B, Proc. Suppl. **18C**, 86 (1990).
- [58] A. Connolly, R. Thorne, and D. Waters, Phys. Rev. D **83**, 113009 (2011).